

Capacity-Approaching Coded-Modulation Schemes

5.9 级联 TCM

TCM 码可以按 Turbo 方式并行级联，也可以与其它码构成串行级联系统（例如，在 RS+TCM 中做内码，在 TCM+STBC 中做外码）。

5.9.1 TCM 码的(Symbol-Based Nonbinary) MAP 译码算法

Consider a general trellis code. Let $\mathbf{u} = (\mathbf{u}_1, \mathbf{u}_2, \dots, \mathbf{u}_N)$ be an information symbol sequence of length N . Each information symbol is assumed to be a binary m -tuple, i.e., $\mathbf{u}_k = (u_{k,0}, u_{k,1}, \dots, u_{k,m-1}) \in \mathbb{F}_2^m$, for $k=1, 2, \dots, N$. For convenience, we will denote \mathbf{u}_k by its decimal representation; i.e., assume $u_k \in \mathcal{U} = \{0, 1, \dots, 2^m - 1\}$. The m -bit symbols are fed into a TCM encoder, producing a sequence of N modulated symbols, $\mathbf{x} = (x_1, x_2, \dots, x_N)$, where $x_k \in \mathcal{X}$ with \mathcal{X} standing for the signal constellation of size $|\mathcal{X}| = 2^n$. We assume that the symbols x_k are transmitted over an AWGN channel. Let $\mathbf{y} = \mathbf{y}_1^N = (y_1, y_2, \dots, y_N)$ be the received sequence, where y_k ($k=1, 2, \dots, N$) is the noisy observation of x_k if x_k is not punctured; otherwise, set $y_k = *$ (implying no observation obtained).

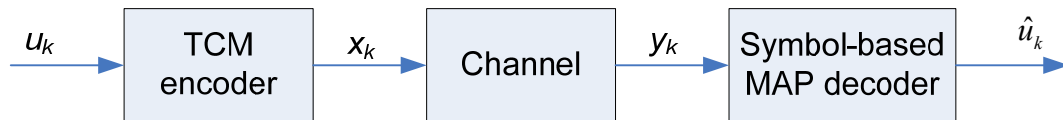


Figure 5.9.1 A trellis coding system

The received sequence is fed to the TCM decoder to produce the estimate of transmitted 2^m -ary information symbols. To minimize the probability of symbol errors, the symbol-based MAP decoder may be used. This decoder computes the APP for every 2^m -ary information symbol; i.e., $P(u_k = i | \mathbf{y}_1^N)$, for $i = 0, 1, \dots, 2^m - 1, k = 1, 2, \dots, N$. Then it makes decisions according to the MAP criterion:

$$\hat{u}_k = \arg \max_{i \in \mathcal{U}} P(u_k = i | \mathbf{y}_1^N)$$

where $\mathcal{U} = \{0, 1, \dots, 2^m - 1\}$.

We now describe the MAP algorithm in detail by using the trellis diagram. For no loss of generality of the result, we assume that the trellis diagram contains parallel transitions. Refer to Fig. 5.9.2. Denote by \mathcal{S} the set of encoder states and by $M = |\mathcal{S}|$ the number of states. In Fig. 5.9.2 $|\mathcal{S}|=4$ is assumed. Let S_k be the encoder state at time k . A branch at the k th section in the corresponding trellis diagram can be specified by $b \equiv (S_{k-1}, u_k, x_k, S_k)$, where u_k and x_k are the information and modulated symbols associated with the state transition $S_{k-1} \rightarrow S_k$. Denote by $B_k(s', s)$ the set of all the parallel branches connecting $S_{k-1} = s' \in \mathcal{S}$ and $S_k = s \in \mathcal{S}$. The non-binary MAP algorithm can be derived as follows.

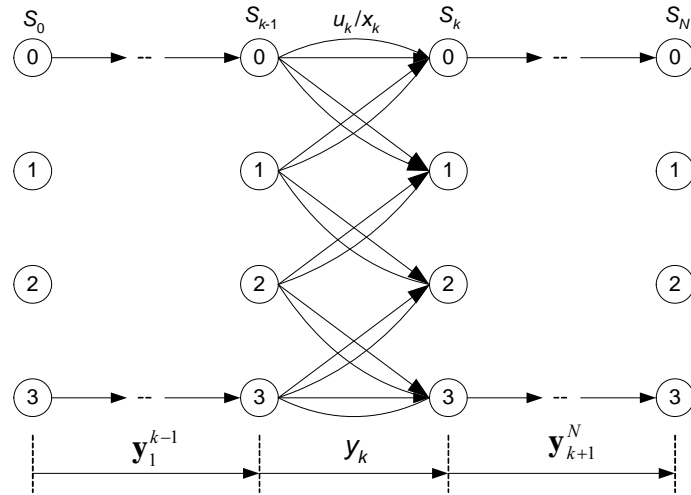


Figure 5.9.2

$$\begin{aligned}
 P(u_k = i | \mathbf{y}_1^N) &= \sum_{\forall (s', s) \in B_k^i} P(u_k = i, S_{k-1} = s', S_k = s | \mathbf{y}_1^N) \\
 &= \sum_{\forall (s', s) \in B_k^i} \frac{p(u_k = i, S_{k-1} = s', S_k = s, \mathbf{y}_1^N)}{p(\mathbf{y}_1^N)} \quad (5.9.1)
 \end{aligned}$$

where B_k^i is the set of transitions $S_{k-1} \rightarrow S_k$ that are caused by the input $u_k=i$. According to the BCJR algorithm, the probabilities $p(u_k = i, S_{k-1} = s', S_k = s, \mathbf{y}_1^N)$ can be calculated as

$$p(u_k = i, S_{k-1} = s', S_k = s, \mathbf{y}_1^N) = \alpha_{k-1}(s') \cdot \gamma_k^i(s', s) \cdot \beta_k(s)$$

where

$\alpha_k(s) \equiv p(S_k = s, \mathbf{y}_1^k)$ is the forward state metric;

$\beta_k(s) \equiv p(\mathbf{y}_{k+1}^N | S_k = s)$ is the backward state metric; and

$\gamma_k^i(s', s) \equiv p(u_k = i, S_k = s, \mathbf{y}_k | S_{k-1} = s')$ is the metric of the trellis branch b connecting $S_{k-1} = s'$ to $S_k = s$ with $u_k = i$.

Note that we do not necessarily need the exact values of $P(u_k = i | \mathbf{y}_1^N)$, but only their ratios.

Since for a fixed k , the vector $P(u_k = i | \mathbf{y}_1^N)$, being a probability vector, must sum to unity,

thus by normalizing the sum to unity, we can omit the constant factor $\frac{1}{p(\mathbf{y}_1^N)}$ in (5.9.1) and

use the following simplified expression:

$$P(u_k = i | \mathbf{y}_1^N) \propto \sum_{\forall (s', s) \in B_k^i} \alpha_{k-1}(s') \cdot \gamma_k^i(s', s) \cdot \beta_k(s)$$

Now we consider the calculation of the branch metric $\gamma_k^i(s', s)$, which is the key point of the symbol-based MAP algorithm, and is also the primary difference between the MAP algorithm for binary turbo codes and the algorithm under consideration.

Using Bayes' rule, the term $\gamma_k^i(s', s)$ can be written as

$$\begin{aligned} \gamma_k^i(s', s) &= p(\mathbf{y}_k | S_k = s, S_{k-1} = s', u_k = i) \cdot P(S_k = s | S_{k-1} = s', u_k = i) \cdot P(u_k = i | S_{k-1} = s') \\ &= p(y_k | x_k) \cdot P(u_k = i) \cdot P(S_k = s | S_{k-1} = s', u_k = i) \end{aligned} \quad (5.9.2)$$

where $p(y_k | x_k)$ is the probability of receiving y_k given the transmitted symbol x_k , $P(u_k)$

is the *a priori* probability of $u_k = i$, and $P(S_k = s | S_{k-1} = s', u_k = i)$ is 1 or 0, indicating

whether or not a state transition $S_{k-1} \rightarrow S_k$ with input $u_k = i$ exists. Thus, for a trellis branch

b , we have

$$\gamma_k^i(s', s) = \begin{cases} P(u_k), & \text{if } y_k = * \\ p(y_k | x_k) \cdot P(u_k), & \text{otherwise} \end{cases} \quad (5.9.3)$$

Define

$$\gamma_k(s', s) \equiv p(S_k = s, \mathbf{y}_k | S_{k-1} = s')$$

$$= \sum_{\forall b_k \in B_k(s',s)} \gamma_k^i(s',s)$$

which represent the combined branch metrics. Then the non-binary BCJR algorithm can be summarized as follows.

Forward recursion:
$$\alpha_k(s) = \sum_{s' \in \mathcal{S}} \alpha_{k-1}(s') \gamma_k(s',s) \quad (5.9.4)$$

Backward recursion:
$$\beta_{k-1}(s') = \sum_{s \in \mathcal{S}} \beta_k(s) \gamma_k(s',s) \quad (5.9.5)$$

Output:
$$P(u_k = i | \mathbf{y}_1^N) \propto \sum_{\forall (s',s) \in B_k^i} \alpha_{k-1}(s') \cdot \gamma_k^i(s',s) \cdot \beta_k(s) \quad (5.9.6)$$

The boundary conditions are the same as for the binary turbo codes. For numerical stability, it is necessary to control the dynamic range of the likelihood terms computed in (5.9.4) to (5.9.6). This can be performed by normalizing the sum of the $\alpha_k(s)$ and the $\beta_k(s)$ values to unity at every particular k symbol. Of course, the algorithm can also be implemented in the log-domain with reduced computational complexity, resulting in the Log-MAP or Max-Log-MAP version.

5.9.2 Turbo Trellis-Coded Modulation (TTCM)

TTCM 是由两个（或多个）TCM 码按照 Turbo 码的方式级联起来构成的并行级联编码调制系统，它是标准二元 turbo 码的直接推广。This technique was originally proposed by Robertson and Worz in 1996 [?].

5.9.2.1 TTCM Encoder

A TTCM encoder consists of the parallel concatenation of two (or multiple) trellis-coded modulation (TCM) schemes in the same fashion as binary turbo codes. Each component TCM encoder consists of a convolutional encoder of rate $m/(m+1)$ and a signal mapper. The mapping of coded bits to signal points follows the Ungerboeck's rule of mapping by set partitioning. The first TCM encoder operates on the original input bit sequence, while the second TCM encoder manipulates the interleaved version of the input bit sequence. Here, the interleaving works on groups of bits instead of individual bits. See Fig. 5.9.3, where a symbol-based odd-even interleaver is assumed. To avoid excessive rate loss, a special puncturing technique is used: Symbols from a 2^{m+1} -ary signal constellation are transmitted alternately from the first and second encoders; i.e., the puncturing matrix is given by

$$P = \begin{bmatrix} 1 & 0 \\ 0 & 1 \end{bmatrix}$$

Thus each information bit pair is transmitted in exactly one transmitted symbol with the parity bit alternately chosen from the first and second encoders.

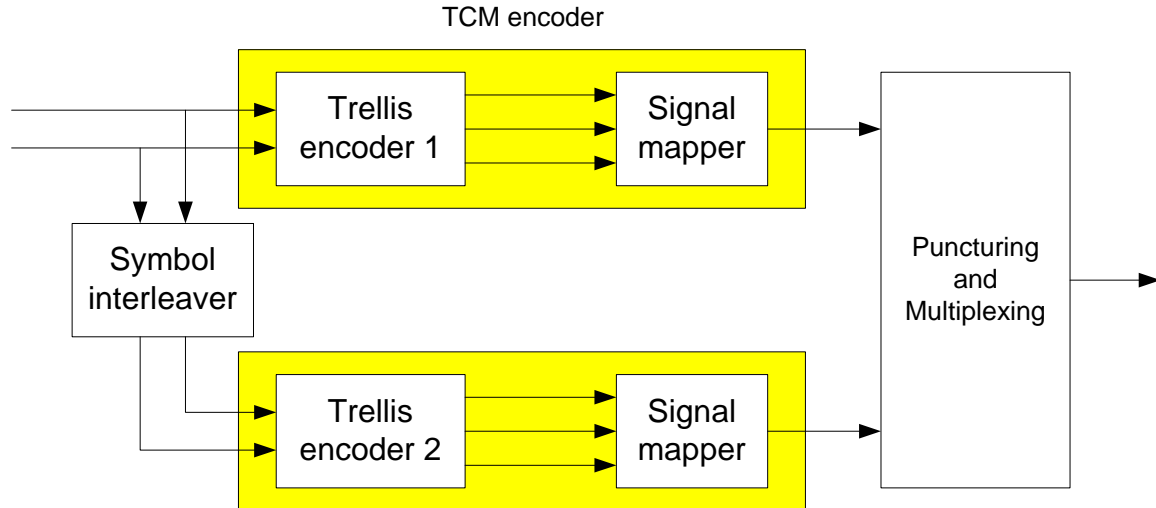


Figure 5.9.3 TTCM encoder. The puncturer is used to avoid rate loss by enabling the transmission of signals carrying the same information bits only once.

Assume that a D -dim constellation is used. At each step, m information bits are input to the TTCM encoder and then a modulated symbol selected from a D -dim signal constellation of size 2^{m+1} is transmitted. This yields a throughput of $2m/D$ bits per 2-dim symbol.

We now consider the above odd-even interleaving-puncturing rule more 更深入、更一般地. Let L denote the number of component codes used in a parallel concatenated system. Then the above odd-even interleaving-puncturing rule may be expressed mathematically via introducing the following definitions.

Definition: A (pseudo-random) interleaver satisfying the following constraint is called a modulo- L interleaver:

$$\pi(k) \bmod L = k \bmod L,$$

where k stands for the symbol position before interleaving.

Definition: A modulo- L puncturer is one that punctures all the modulated symbols in the l th component code, except those at position $\{k \mid k \bmod L = l\}$.

For a TTCM scheme, the modulo- L interleaving together with the modulo- L puncturing rule ensure that one and only one modulated symbol carrying the same u_k is transmitted, and that the punctured symbols are uniformly distributed in each component code. It is clear that when $L=2$, the above modulo- L interleaving-puncturing rule is equivalent to that used in [3].

As an example, Fig.5.9.4 shows an 8-state TTCM encoder for 8-PSK.

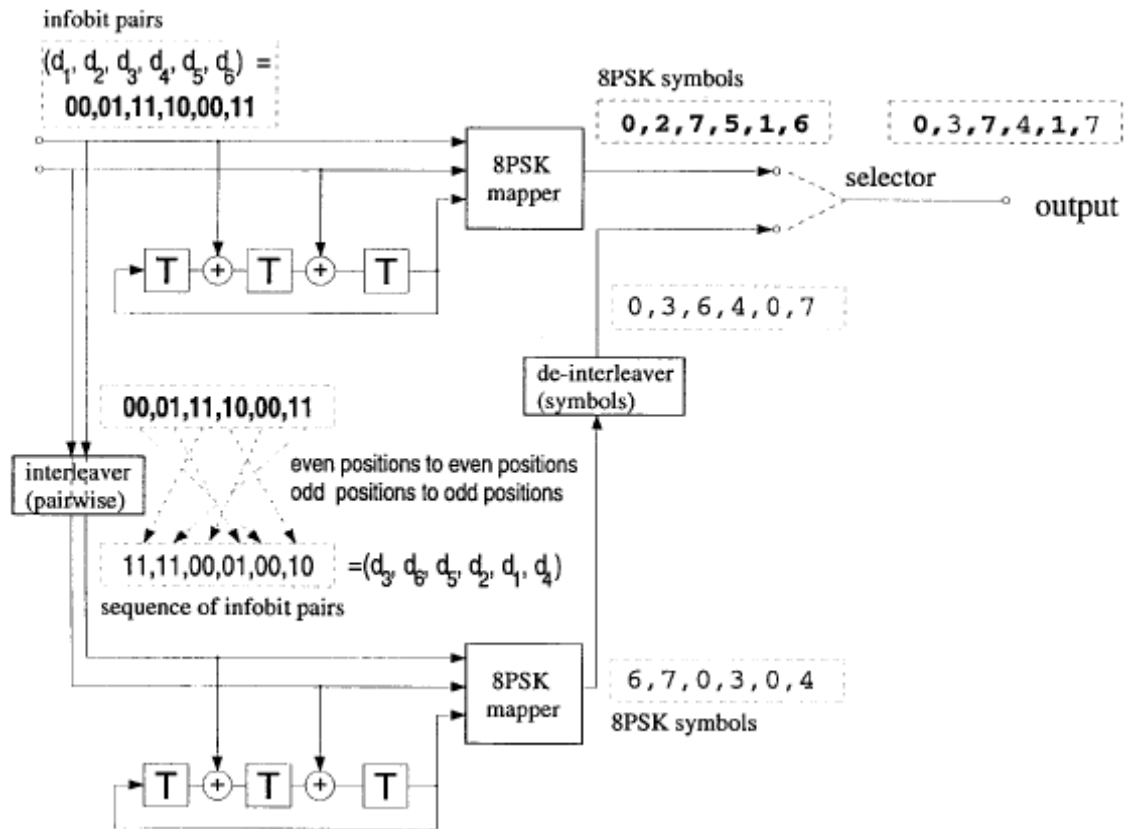


Figure 5.9.4 From [Robertson98]

Table 5.9.1 lists the generator polynomials of some component TCM codes that can be employed in the TCM scheme. These polynomials were obtained by Robertson and Worz using an exhaustive computer search method. In Table 5.9.1, \tilde{m} denotes the number of information bits to be encoded from the m information bits contained in an input symbol.

“PUNCTURED” TCM CODES WITH BEST MINIMAL DISTANCE FOR 8-PSK AND QAM (IN OCTAL NOTATION)

Code	\tilde{m}	$H^0(D)$	$H^1(D)$	$H^2(D)$	$H^3(D)$	$d_{\text{free}}^2 / \Delta_0^2$
2-dim. 8-PSK, 8 states	2	11	02	04		3
4-dim. 8-PSK, 8 states	2	11	06	04		3
2-dim. 8-PSK, 16 states	2	23	02	10		3
4-dim. 8-PSK, 16 states	2	23	14	06		3
2-dim. Z^2 , 8 states	3	11	02	04	10	2
2-dim. Z^2 , 16 states	3	21	02	04	10	3
2-dim. Z^2 , 8 states	2	11	04	02		3
2-dim. Z^2 , 16 states	2	21	04	10		4

5.9.2.2 TCM Decoder

The iterative decoder for TCM is similar to that used to decode binary turbo codes, except that there is a difference in the nature of the information passed from one decoder to the other. Fig. 5.9.5 illustrates the concept of *a priori*, *a posteriori* and extrinsic information used in TCM decoder.

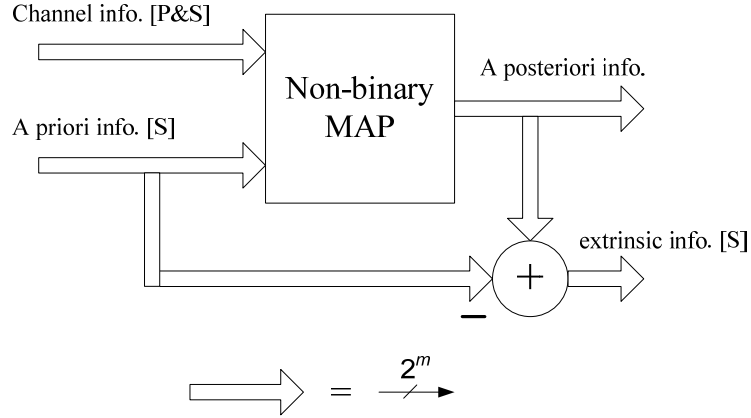


Figure 5.9.5. Schematic of the component decoders for TTCM codes

Note that in a symbol-based nonbinary TTCM scheme, the m systematic information bits and the parity bit are transmitted together in the same modulated symbol. Hence, the systematic component (corresponding received systematic value in binary turbo decoder) of the non-binary symbol cannot be separated from the extrinsic component. In this scenario the symbol-based information can be split into only two components: L_a and $L_{e\&s}$. Each decoder passes only the latter information to the next component decoder while the *a priori* information is removed at each component decoder's output.

The complete TTCM decoder operating in the log domain is depicted in Fig. 5.9.6. At the beginning of decoding, the received symbols are input to the "metric" block so as to generate a set of $M=2^{m+1}$ symbol likelihoods. The selector switches select the current symbol's reliability metric produced by the "metric block" if the current symbol was not punctured by the corresponding encoder. Otherwise puncturing will be applied where the likelihoods of the various legitimate symbols at index k are set to 0 in the log-domain. That is 初始化

$$L_{p\&s,k} = \begin{cases} \log p(y_k | x_k), & \text{for un-punctured symbols} \\ 0, & \text{for punctured symbols} \end{cases}$$

On this basis, the TTCM decoder operates according to the "turbo principle".

Specifically, for the MAP decoder 1, if the modulated symbol from the component TCM encoder 1 is punctured at time k , then $y_k = *$ for decoder 1, and set $L_{p\&s} = 0$. The only input is *a priori* information $L_a^{(1)} = \tilde{L}_{e\&s}^{(2)}$ from the other component decoder, and this includes the systematic information for u_k . At the output of the MAP decoder 1, the *a priori* information is subtracted from the *a posteriori* information, so that the same information is not used more than once in the other component decoder. Thus, the information passed from the decoder 1 to the decoder 2, $L_e = L - L_a$, contains only the extrinsic information on u_k .

If the modulated symbol from the component TCM encoder 1 is not punctured at time k , then $L_{p\&s} \triangleq \log p(y_k | x_k)$ represents the channel information, and the information passed from the decoder 1 to the decoder 2, $L_e = L_{e\&s}$, contains the inseparable *extrinsic* as well as

systematic information component on u_k .

The decoder 2 operates according to the same message-passing principle as above.

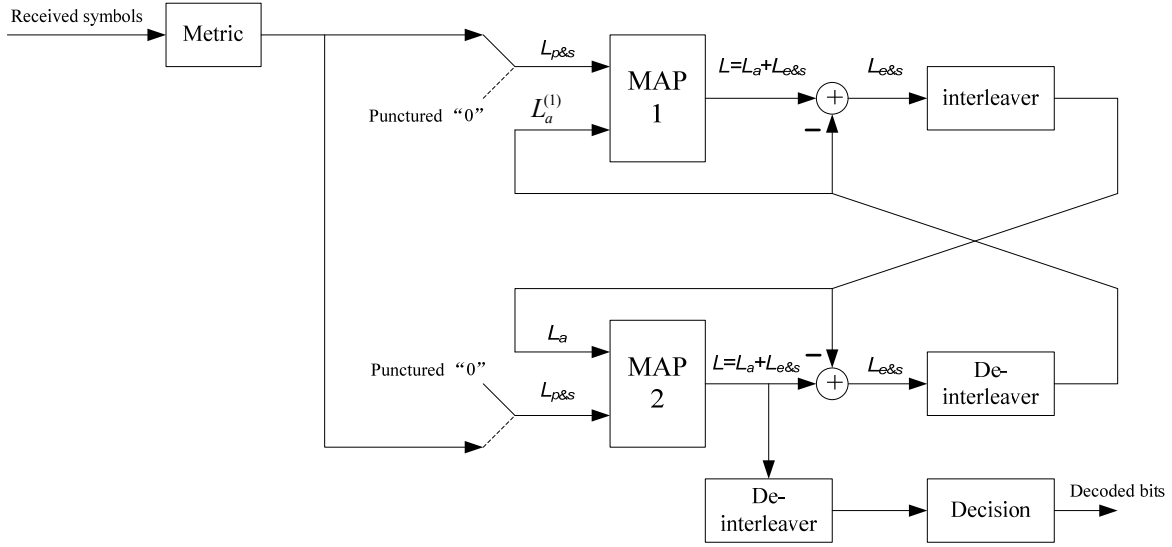


Figure 5.9.6 Structure of the TTCM decoder.

5.9.2.3 Numerical results

5.9.3 Concatenated Two-State TCM (CT-TCM) Schemes

5.9.3.1 Encoder

The component encoder of a CT-TCM code consists of a binary two-state trellis encoder followed by a multi-ary signal mapper, see Fig. 5.9.7. Let a binary n -tuple $\mathbf{d}_k = (d_{k,0}, \dots, d_{k,n-1})$ be an information symbol. Let $\mathbf{d} = \{\mathbf{d}_k, k \geq 0\}$ be an input sequence to the binary encoder, producing a coded symbol sequence $\mathbf{c} = \{\mathbf{c}_k\}$. Each \mathbf{c}_k contains a parity check bit q_k , i.e., $\mathbf{c}_k = (\mathbf{d}_k, q_k)$, and is mapped to an appropriate 2^{n+1} -ary signal constellation, producing a modulated symbol x_k . In the following, \mathbf{c} and $\mathbf{x} = \{x_k\}$ are also referred to as unmodulated and modulated codewords, respectively.

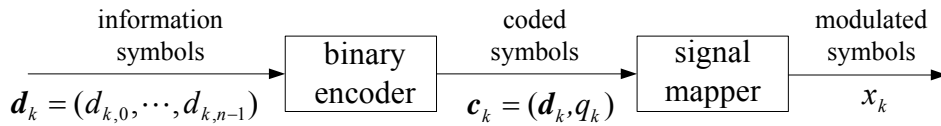


Fig. 5.9.7. The component encoder structure for the CT-TCM scheme.

We assume that the binary encoder in Fig. 5.9.7 is characterized by the two-state trellis in Fig. 5.9.8 (similar to the tree encoder in [Liping2001]). The parity check bit q_k is generated by

$$q_k = q_{k-1} + \mathbf{d}_k \cdot \mathbf{g}_k = \sum_{i=0}^k d_i \cdot g_i \quad \text{mod } 2, \quad k > 0 \quad (5.9.7)$$

with $q_0 = \mathbf{d}_0 \cdot \mathbf{g}_0$. Here $\mathbf{g}_k = (g_{k,0}, g_{k,1}, \dots, g_{k,n-1})^T$ is an indication vector defined by

$$\mathbf{g}_{k,j} = \begin{cases} 1 & \text{if } d_{k,j} \text{ participates in parity check} \\ 0 & \text{otherwise} \end{cases} \quad (5.9.8)$$

The code in Fig. 5.9.8 is completely specified by $\{\mathbf{g}_k\}$.

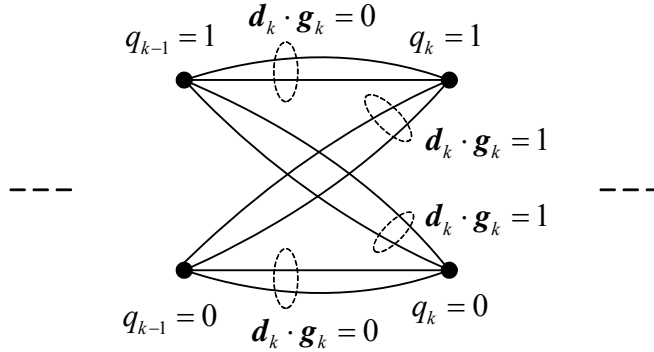


Fig. 5.9.8. A two-state trellis diagram with 2^{n+1} branches in a trellis section. (In this figure, $n=2$.)

■ The Global Encoder of CT-TCM Scheme

Fig. 5.9.9 depicts a global CT-TCM scheme, where M component encoders are concatenated in parallel by M symbol-interleavers. Modulo- M interleavers satisfying the following constraints are assumed,

$$\pi^{(m)}(k) \bmod M = k \bmod M, \quad \text{for } m = 0, 1, \dots, M-1$$

In order to increase spectral efficiency, we puncture all the modulated symbols in the m th component code, except those at position $\{k \mid k \bmod M = m\}$. This, together with the constraint in (3), ensures that one and only one modulated symbol carrying the same \mathbf{d}_k is transmitted, and that the punctured symbols are uniformly distributed in each component code. We will always assume that a signal constellation of size 2^{n+1} is used. This yields a spectral efficiency of n bits per symbol.

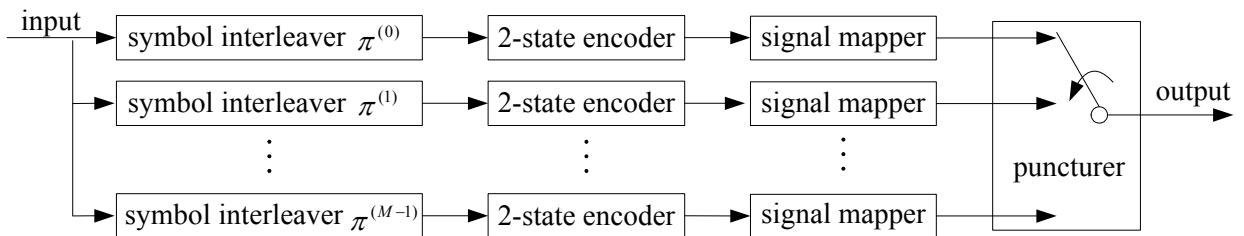


Fig. 5.9.9. A global CT-TCM encoder structure.

5.9.3.2 Decoder

The CT-TCM decoder structure is based on the multi-dimensional turbo-decoder incorporating the BCJR algorithm. The global decoder operating in the log domain for a CT-TCM code is shown in Fig. 5.9.10. It consists of M local APP (*a posteriori* probability) decoders, each for one component code. The variables involved in Fig. 5.9.10 are the log-likelihood (LL) values, as detailed below.

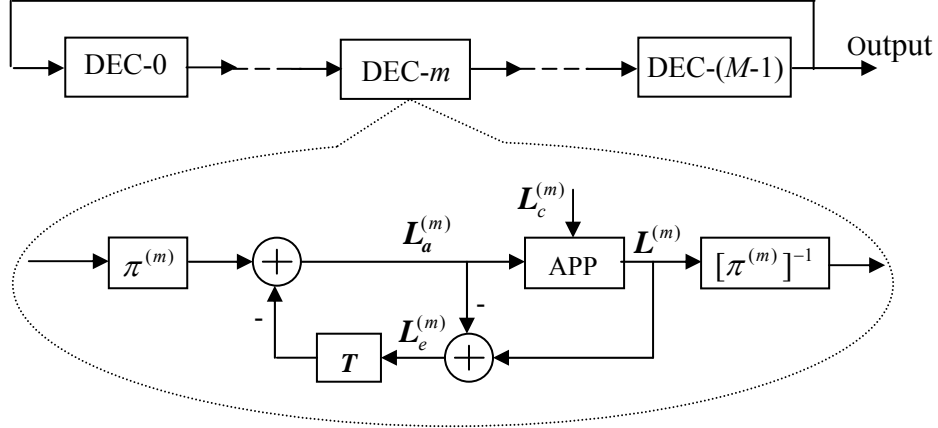


Fig. 5.9.10. The global decoder: “ T ” for delay of one iteration and “ π ” for interleaving.

$\mathbf{L}^{(m)}$ the *a posteriori* LL values for all information symbols after decoding the m th component code.

$\mathbf{L}_c^{(m)}$ the LL values $\{\log p(y_k | x_k)\}$ based on individual channel observations of the m th component code. Its elements $\{L_{c,k}^{(m)}\}$ are calculated as

$$L_{c,k}^{(m)} = \begin{cases} \log p(y_k | x_k), & \text{for un - punctured symbols} \\ 0, & \text{for punctured symbols} \end{cases}$$

$\mathbf{L}_a^{(m)}$ the *a priori* LL values for all information symbols for the m th component code. It is initialized to zeroes, implying no *a priori* information.

$\mathbf{L}_e^{(m)}$ the extrinsic information produced by the m th component code, defined by

$$\mathbf{L}_e^{(m)} = \mathbf{L}^{(m)} - \mathbf{L}_a^{(m)}.$$

The M local decoders operate successively. $\mathbf{L}_a^{(m)}$ contains the accumulated extrinsic information generated by all the local decoders except DEC- m ,

$$\mathbf{L}_a^{(m)} = \underbrace{\mathbf{L}_e^{(m+1)} + \mathbf{L}_e^{(m+2)} \dots + \mathbf{L}_e^{(M-1)}}_{\text{from the previous iteration}} + \underbrace{\mathbf{L}_e^{(0)} + \mathbf{L}_e^{(1)} + \dots + \mathbf{L}_e^{(m-1)}}_{\text{from the current iteration}}$$

It is used together with channel observations $L_c^{(m)}$ in the next APP decoding of the m th component code. A discussion on this global decoder can also be found in [16].

5.9.4 PC-TCM

In this scheme, two parallel concatenated rate $k/(k+1)$ convolutional codes use all their information bits to produce the parity bit which is sent to their respective symbol mappers, but the information bits are punctured in such a fashion that one half of them are used in the first trellis code and the other half in the second trellis code [Benedetto-Divsalar96]. This is done to limit the number of points in the signal constellation to $2^{(k/2)+1}$. Also, the information bits transmitted by the two trellis encoders are interleaved by different bit interleavers (see Figure 5.9.11). In [Fragouli-Wesel01], a variation of this scheme is presented where a symbol interleaver is used instead of bit interleavers, resulting in improved BER performance in the waterfall region.

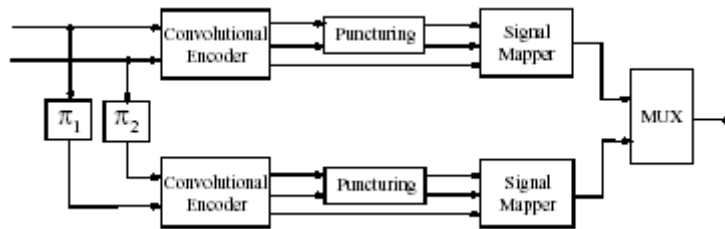
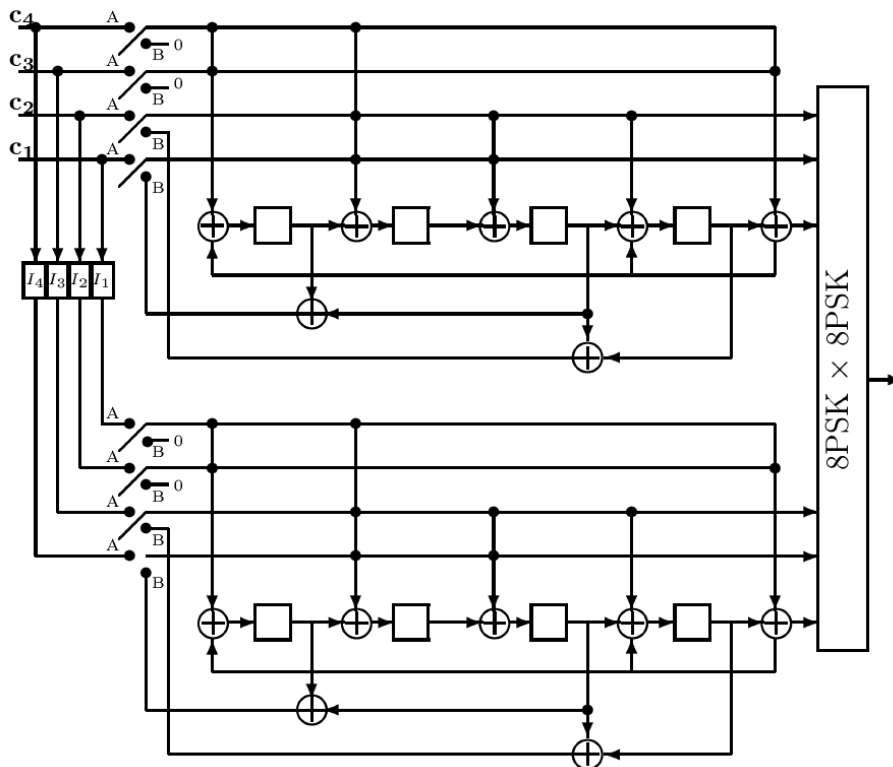


Figure 5.9.11



5.10 Multilevel Codes and Multistage Decoding

MLC was first proposed by Imai and Hirakawa in 1977, with the idea of protecting each

address bit $c^{(i)}$ of the signal point by an individual binary code C_i at level i . The individual codes were chosen in such a way that the minimum distance of the Euclidean space code was maximized. This is now known as balanced distance rule. At the receiver side, each code C_j is decoded individually starting from the lowest level and taking into account decisions of prior decoding stages. This is known as multistage decoding.

Compared with TCM, the MLC approach provides flexible transmission rates; any code (e.g., block codes, convolutional codes, or concatenated codes) can be used as component code. TCM can be viewed as a special case of MLC using a single convolutional code with a nonbinary output alphabet while higher levels remain uncoded.

5.10.1 Block coded modulation (BCM)

BCM is an example of multilevel coded modulation. 从 TCM 的 set-partitioning 可以看出, 信号 label 中的不同 bit 要求不同的保护能力。在 BCM 中, we provide this by 用不同纠错能力的码编不同 bit. 具体地说, encode the LSB with a powerful code, and encode the MSB with the least powerful code (甚至不编码)。

将 label 排成一个阵列, forming columns with LSB at the top.

$$\begin{bmatrix} \mathbf{a} \\ \mathbf{b} \\ \mathbf{c} \end{bmatrix} = \begin{bmatrix} a_0 & a_1 & \cdots & a_{n-1} \\ b_0 & b_1 & \cdots & b_{n-1} \\ c_0 & c_1 & \cdots & c_{n-1} \end{bmatrix}$$

$$\Rightarrow \mathbf{x} = [x_0 \quad x_1 \quad \cdots \quad x_{n-1}]$$

Vectors \mathbf{a} , \mathbf{b} , and \mathbf{c} should form 三个不同的长为 n 的码。

As an example, Fig. 5.10.1 shows a 3-level BCM code over the 8-PSK signal set.

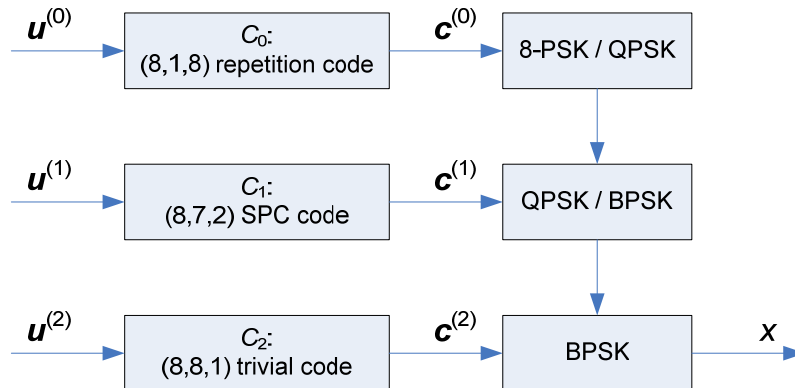


Fig. 5.10.1

An l -level BCM code over a signal set (M-PSK or M-QAM) with 2^l signal points is constructed in the same manner as a 3-level 8-PSK BCM code. For $0 \leq i < l$, let C_i be a binary (n, k_i, d_i) linear block code of length n , dimension k_i , and minimum Hamming distance d_i . Let

$$\begin{aligned}
\mathbf{c}^{(0)} &= (c_0^{(0)}, c_1^{(0)}, \dots, c_{n-1}^{(0)}) \\
\mathbf{c}^{(1)} &= (c_0^{(1)}, c_1^{(1)}, \dots, c_{n-1}^{(1)}) \\
&\vdots \\
\mathbf{c}^{(l-1)} &= (c_0^{(l-1)}, c_1^{(l-1)}, \dots, c_{n-1}^{(l-1)})
\end{aligned}$$

be l codewords in $\mathcal{C}_0, \mathcal{C}_1, \dots, \mathcal{C}_{l-1}$, respectively. Forming the following sequence

$$\mathbf{c}^{(0)} * \mathbf{c}^{(1)} * \dots * \mathbf{c}^{(l-1)} = (c_0^{(0)} c_0^{(1)} \dots c_0^{(l-1)}, \dots, c_j^{(0)} c_j^{(1)} \dots c_j^{(l-1)}, \dots, c_{n-1}^{(0)} c_{n-1}^{(1)} \dots c_{n-1}^{(l-1)})$$

For $0 \leq j < n$, we take $c_j^{(0)} c_j^{(1)} \dots c_j^{(l-1)}$ as the label of a signal point $a \in \mathcal{X}$. Then

$$\begin{aligned}
f(\mathbf{c}^{(0)} * \mathbf{c}^{(1)} * \dots * \mathbf{c}^{(l-1)}) &= (f(c_0^{(0)} c_0^{(1)} \dots c_0^{(l-1)}), \dots, f(c_j^{(0)} c_j^{(1)} \dots c_j^{(l-1)}), \dots, f(c_{n-1}^{(0)} c_{n-1}^{(1)} \dots c_{n-1}^{(l-1)})) \\
&= (x_0, x_1, \dots, x_{n-1})
\end{aligned}$$

is a sequence of n signals, with $x_j = f(c_j^{(0)} c_j^{(1)} \dots c_j^{(l-1)}) \in \mathcal{X}$. Then

$$\mathcal{C} \triangleq f(\mathcal{C}^{(0)} * \mathcal{C}^{(1)} * \dots * \mathcal{C}^{(l-1)}) = \left\{ f(\mathbf{c}^{(0)} * \mathbf{c}^{(1)} * \dots * \mathbf{c}^{(l-1)}) \mid \mathbf{c}^{(i)} \in \mathcal{C}_i \text{ for } 0 \leq i < l \right\}$$

is an l -level BCM code over \mathcal{X} with dimension $k = k_0 + k_1 + \dots + k_{l-1}$.

5.10.2 MLC

MLC is BCM 的推广。分量码不必是等长的二进制线性分组码，也可以是卷积码、级联码甚至非二进制码。它的编码器的一般结构如图 5.10.2 所示。A generic MLC encoder is shown in Fig.5.10.2. A block of K binary source data symbols, $\mathbf{u} = (u_1, u_2, \dots, u_K), u_k \in \{0, 1\}$, is partitioned into l blocks:

$$\mathbf{u}^{(i)} = (u_1^{(i)}, u_2^{(i)}, \dots, u_{K_i}^{(i)}), i = 0, \dots, l-1$$

of length K_i with $\sum_{i=0}^{l-1} K_i = K$. Each data block $\mathbf{u}^{(i)}$ is fed into an individual binary encoder

ENC_i , producing codewords $\mathbf{c}^{(i)} = (c_0^{(i)}, \dots, c_{n-1}^{(i)})$ of the component code \mathcal{C}_i . For simplicity, we

have assumed equal code lengths n at all levels, but in principle the choice of component

codes is arbitrary. The code symbols $\mathbf{c}_j = \{c_j^{(i)}, 0 \leq i < l\}$ at time j is mapped to the signal

constellation, producing the transmitted signal $x_j = f(\mathbf{c}_j) = f(c_j^{(0)} c_j^{(1)} \dots c_j^{(l-1)}) \in \mathcal{X}$. 通常，调

制器使用 Ungerboeck's mapping by set-partitioning 完成信号的映射。

The code rate of \mathcal{C} is given by

$$R = \sum_{i=0}^{l-1} R_i = \sum_{i=0}^{l-1} \frac{K_i}{n} = \frac{K}{n} \quad (5.10.1)$$

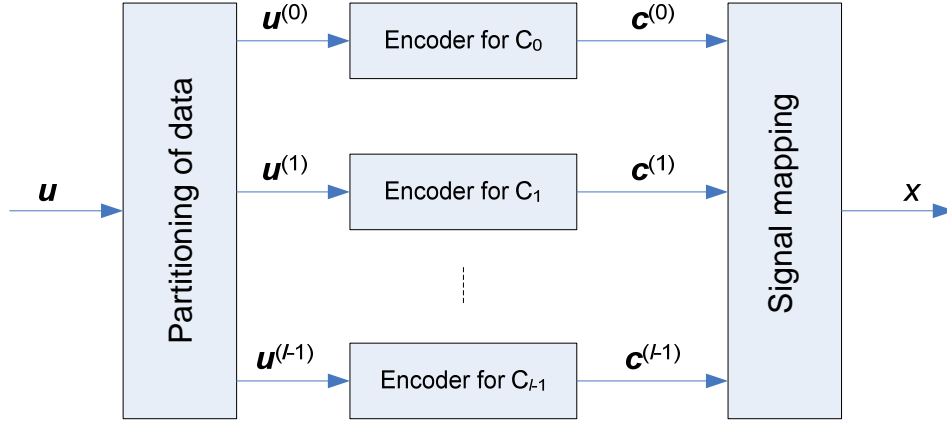


Figure 5.10.2. MLC encoder

- **Information-theoretic considerations:** MLC approach (together with its MSD procedure) is a straightforward consequence of the chain rule of mutual information.

Consider a MLC scheme with l levels. Assume that a binary code is used as a component code at each level, and 调制器使用 Ungerboeck's 子集划分方法进行二进制 label 向量 $\mathbf{c} = (c^{(0)}, c^{(1)}, \dots, c^{(l-1)})$ 到信号点 x 的映射。

At partition level i , the subset $\mathcal{X}(c^{(0)} \dots c^{(i-1)})$ are iteratively divided into two further subsets $\mathcal{X}(c^{(0)} \dots c^{(i-1)} 0)$ and $\mathcal{X}(c^{(0)} \dots c^{(i-1)} 1)$ at level $i+1$:

$$\mathcal{X}(c^{(0)} \dots c^{(i-1)} c^{(i)}) = \{x = f(\mathbf{c}) \mid \mathbf{c} = (c^{(0)} \dots c^{(i)} b^{(i+1)} \dots b^{(l-1)}), b^{(j)} \in \text{GF}(2), i+1 \leq j < l\}$$

Since the mapping $f(\cdot)$ is bijective independently of the actual partitioning strategy, the mutual information $\mathcal{I}(\mathcal{X}; Y)$ between the transmitted signal point $x \in \mathcal{X}$ and the received signal point $y \in \mathcal{Y}$ is equal to the mutual information $\mathcal{I}(c^{(0)} \dots c^{(l-1)}; Y)$ between the label vector $\mathbf{c} \in \{0, 1\}^l$ and the received signal point $y \in \mathcal{Y}$.

From the chain rule for mutual information [Gallager68], we have

$$\begin{aligned} \mathcal{I}(\mathcal{X}; Y) &= \mathcal{I}(c^{(0)} \dots c^{(l-1)}; Y) \\ &= \mathcal{I}(c^{(0)}; Y) + \mathcal{I}(c^{(1)}; Y \mid c^{(0)}) + \dots + \mathcal{I}(c^{(l-1)}; Y \mid c^{(0)} \dots c^{(l-2)}) \end{aligned} \quad (5.10.2)$$

This implies that transmission of vectors with binary digits $c^{(i)}, 0 \leq i < l$, over the physical channel can be separated into the parallel transmission of individual digits $c^{(i)}$ over l equivalent channels, provided that $c^{(0)} \dots c^{(i-1)}$ are known. This 基本原理 is illustrated in

Fig.5.10.3 .

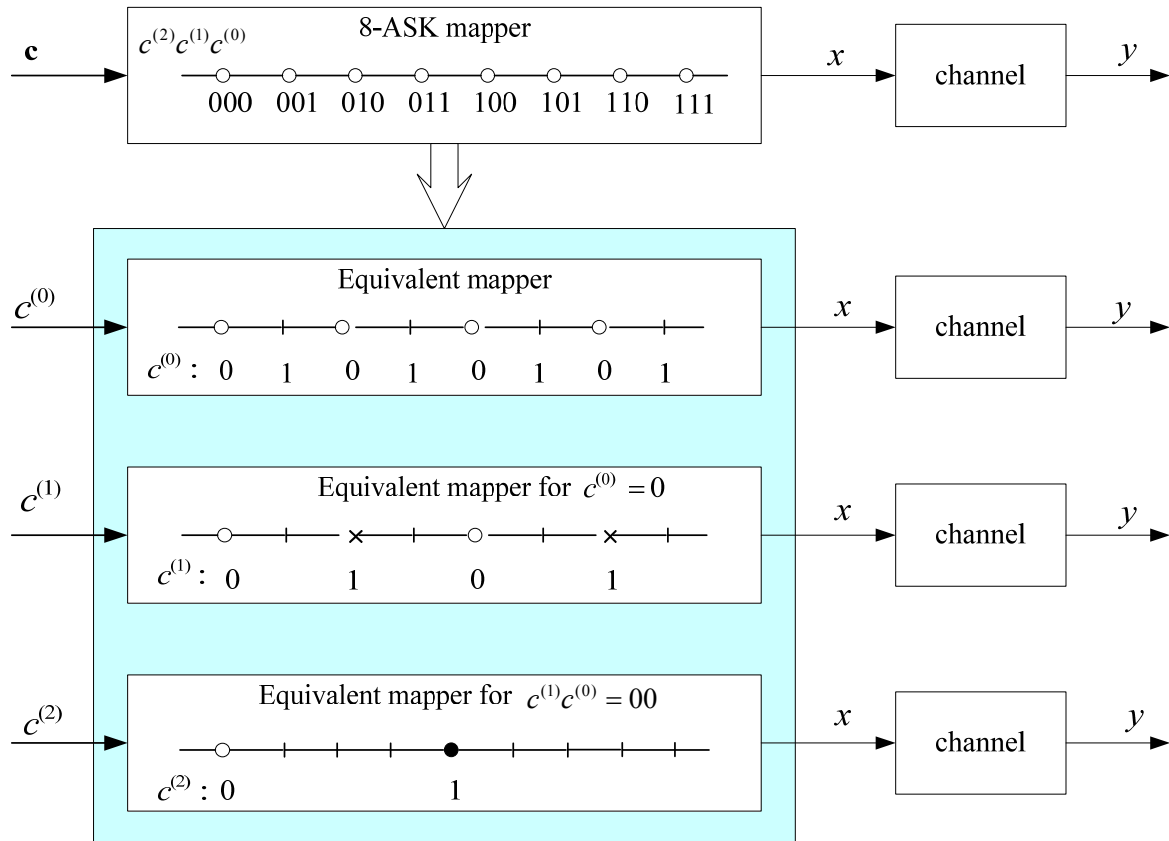


Figure 5.10.3

From the chain rule, the mutual information of the equivalent channel i can be calculated as

$$\mathcal{I}(c^{(i)}; Y | c^{(0)} \dots c^{(i-1)}) = \mathcal{I}(c^{(i)} \dots c^{(l-1)}; Y | c^{(0)} \dots c^{(i-1)}) - \mathcal{I}(c^{(i+1)} \dots c^{(l-1)}; Y | c^{(0)} \dots c^{(i)})$$

where $\mathcal{I}(c^{(i)} \dots c^{(l-1)}; Y | c^{(0)} \dots c^{(i-1)})$ is calculated by averaging over all possible combinations of $c^{(0)} \dots c^{(i-1)}$. (在第 i 层的所有信号子集上求平均)。即

$$\mathcal{I}(c^{(i)} \dots c^{(l-1)}; Y | \underbrace{c^{(0)} \dots c^{(i-1)}}_{\text{Random variables}}) = \mathbf{E}_{c^{(0)} \dots c^{(i-1)}} \left\{ \mathcal{I}(c^{(i)} \dots c^{(l-1)}; Y | \underbrace{c^{(0)} \dots c^{(i-1)}}_{\text{Outcome}}) \right\}$$

等效信道的概念是分析与设计编码调制方案的基本工具。

Thus, the capacity of the equivalent channel is given by

$$C^{(i)} = (c^{(i)}; Y | c^{(0)} \dots c^{(i-1)}) = \mathbf{E}_{c^{(0)} \dots c^{(i-1)}} \left[C(\mathcal{X}(c^{(0)} \dots c^{(i-1)})) \right] - \mathbf{E}_{c^{(0)} \dots c^{(i)}} \left[C(\mathcal{X}(c^{(0)} \dots c^{(i)})) \right]$$

where $C(\mathcal{X}(c^{(0)} \dots c^{(i)}))$ denotes the capacity when using only the subset $\mathcal{X}(c^{(0)} \dots c^{(i)})$ with a priori probabilities $P(a) / P\{\mathcal{X}(c^{(0)} \dots c^{(i)})\}$.

The capacity $C^{(i)}$ 将作为第 i 层分量码的码率设计依据。The total capacity C of a

multilevel coded modulation scheme is then

$$C = \sum_{i=0}^{l-1} C^{(i)}$$

■ Design of multilevel codes:

The essential point for the design of a MLC scheme is the assignment of code rates to the individual coding levels. In [Huber99], five rules are introduced for rate design. For the capacity design rule, the individual rates are chosen to be equal to the capacities of the equivalent channels, i.e.,

$$R_c^{(i)} = C^{(i)}, \quad i = 0, 1, \dots, l-1$$

For the choice of FEC codes, powerful probabilistic coding methods such as turbo codes and LDPC codes are really needed only at the lower levels. At the higher levels, the channels become quite clean and the capacity $C(\Lambda_{i-1}/\Lambda_i)$ approaches $\log_2(\Lambda_{i-1}/\Lambda_i)$, so that the desired redundancy approaches zero. For these levels, algebraic codes and decoding methods may be more appropriate. The state of the art in multilevel coding is reviewed in [Wachsmann99]. Figures 5.10.4-5.10.6 depict the code rate design based on the capacity rule for 8-ASK and 8-PSK MLC schemes.

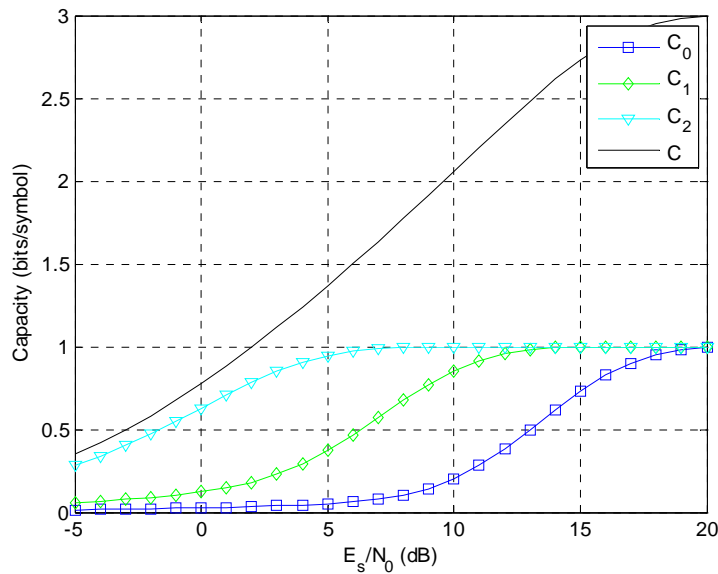
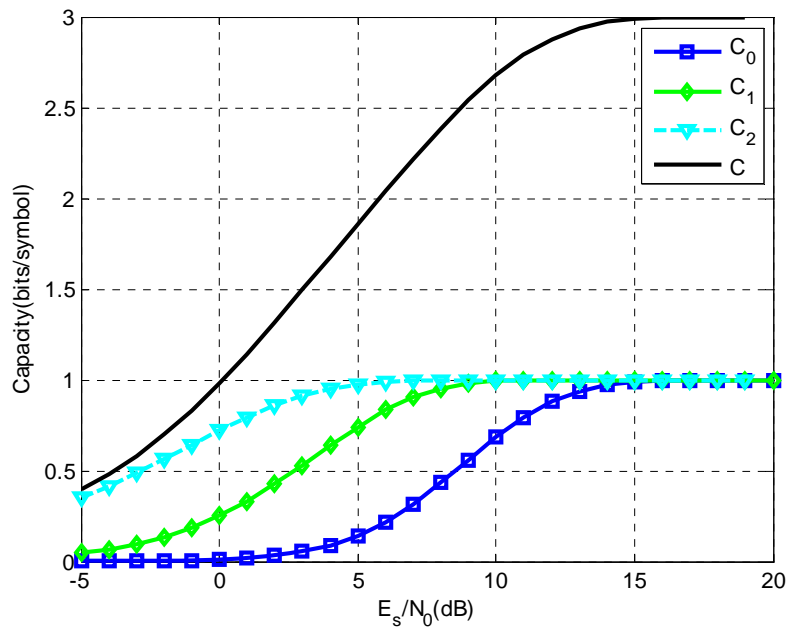
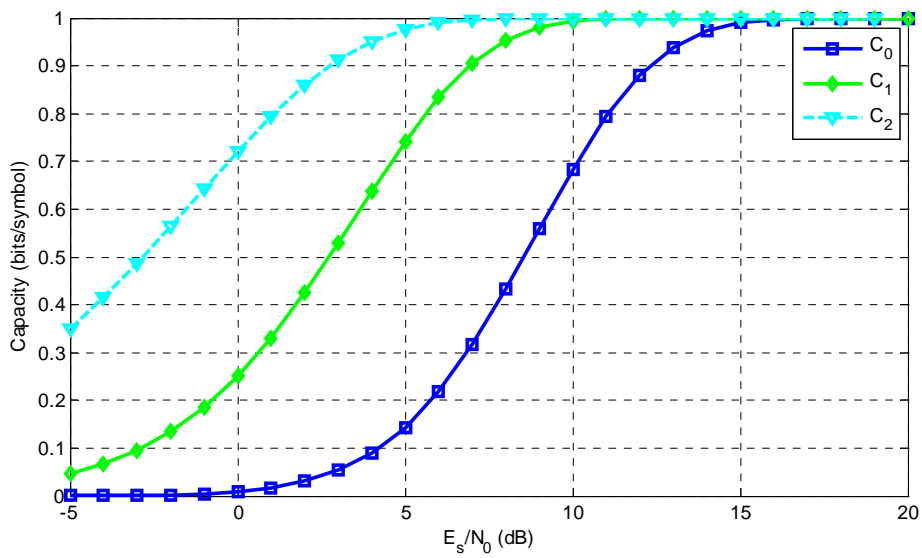


Fig. 5.10.4 采用 8-ASK 的 MLC 系统各层容量



(a)



(b)

Fig. 5.10.5 Capacity of partitioned subsets for 8-PSK modulation (with Ungerboeck partitioning)

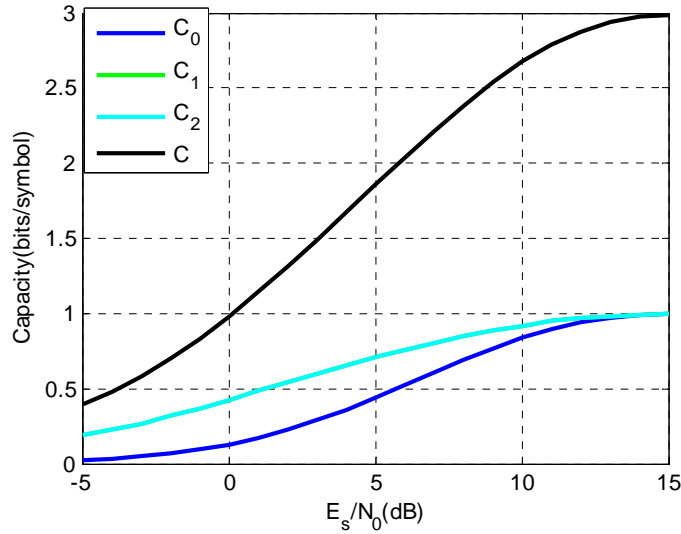


Fig. 5.10.6 Capacity of 8-PSK MLC with Gray mapping (in the figure, $C_1=C_2$)

5.10.3 多级译码 (MSD)

The component codes C_i are successively decoded by the corresponding decoder DEC- i . At stage i , decoder DEC- i processes not only the block $\mathbf{y} = (y_0, \dots, y_{n-1}) \in \mathcal{Y}^N$ of received signal points, but also decision $\hat{c}^{(j)}, 0 \leq j < i-1$ of previous decoding stages j . As long as error-free decisions $\hat{c}^{(j)} = c^{(j)}$ are generated by the decoder DEC- j , MSD can be interpreted as an implementation of the chain rule.

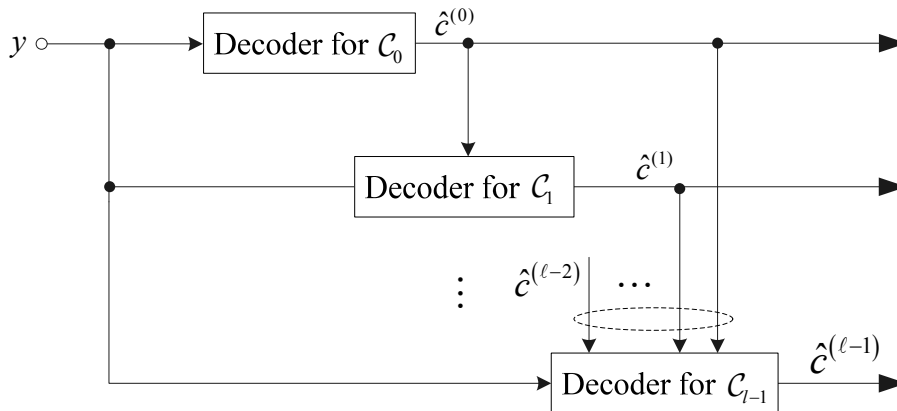


Figure 5.10.7

Note that 尽管 capacity 是相同的 for 不同 labeling strategies, 但是对于 MLC/MSD with finite code length, 不同 labeling strategies (Ungerboeck partitioning, mixed partitioning, Gray labeling) 会影响其 BER 性能。In practice, we recommend MLC schemes based on Ungerboeck set partitioning, where powerful codes with soft-decision decoding are employed

only at lower levels and hard-decision decoding is applied at higher levels.

5.10.4 多层码的迭代译码

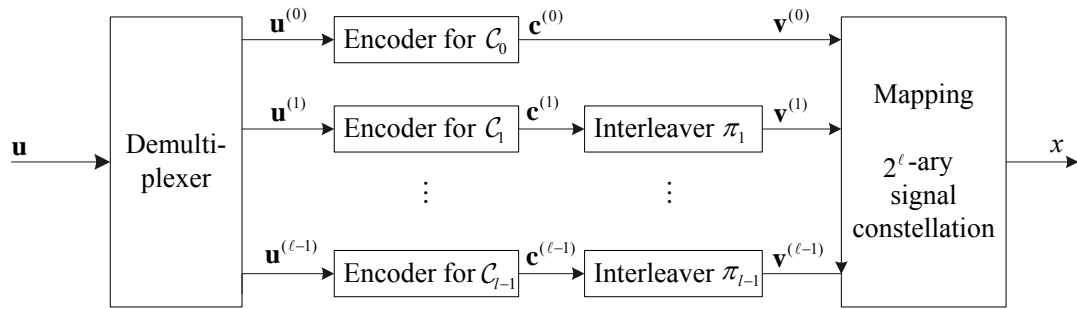
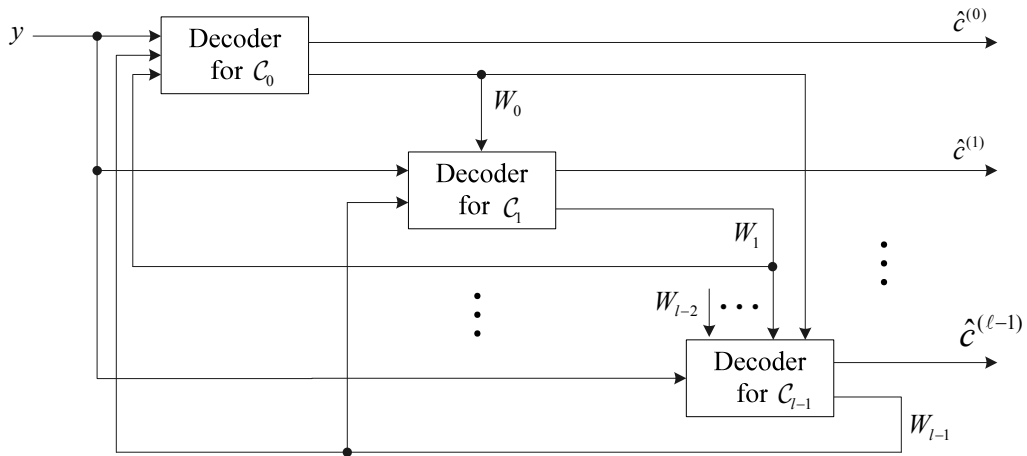
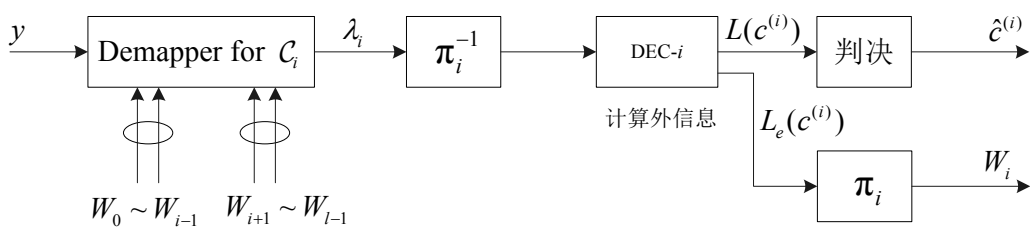


Figure 5.10.8 Encoder



(a) 迭代多级译码器



(b) 第 i 级分量译码器结构

Figure 5.10.9 MLC 的迭代译码

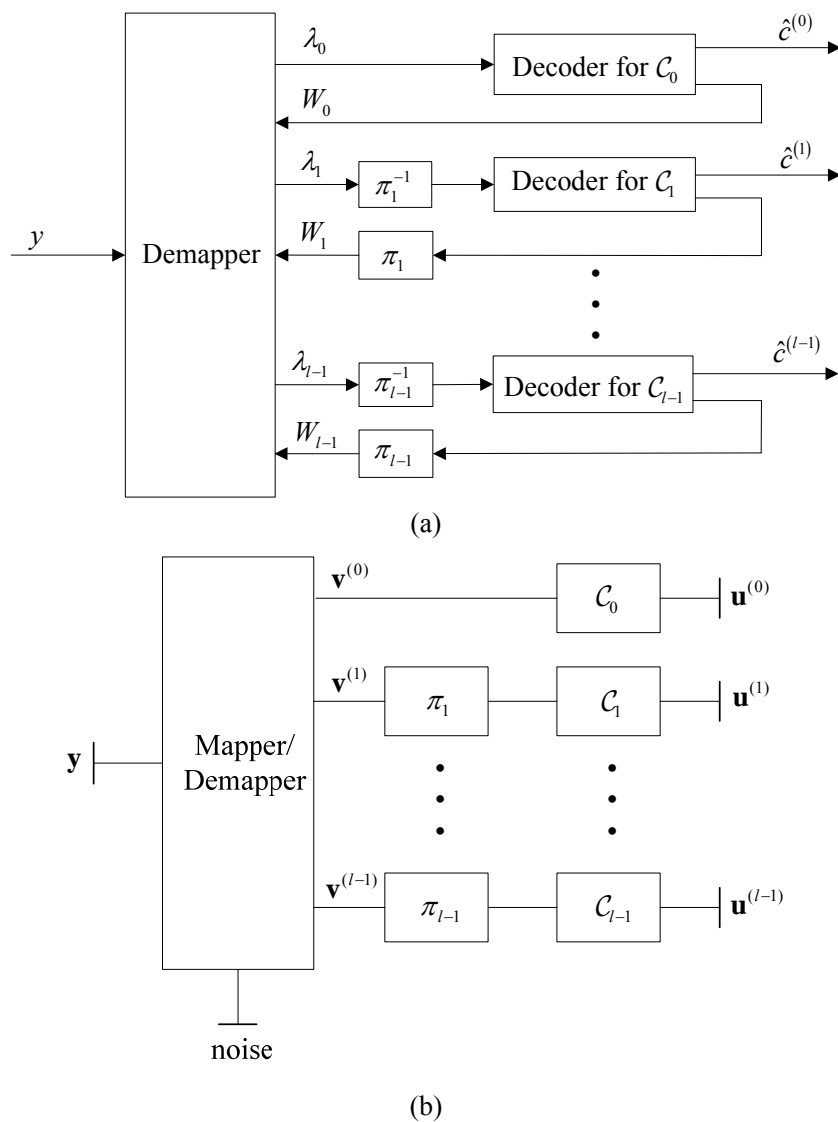


Figure 5.10.10 将各级的 demapper 综合在一起的 Decoder (a)译码器结构框图 (b) Normal graph

5.11 Bit-Interleaved Coded Modulation (BICM) with Iterative Decoding

BICM was first developed by Zehavi primarily for fading channels with the aim of increasing the diversity order of Ungerboeck's TCM schemes, but has turned out to be capable of approaching the capacity of high-SNR AWGN channels as well. Fig. 5.11.1 depicts the coded modulation schemes for fading channels. In Fig. 5.11.1 (a), the channel interleaver is of symbol-based, which can also be placed between the convolutional encoder and signal mapper. The symbols are interleaved with a depth exceeding the coherent time of the fading process. Fig. (b) is the original BICM scheme proposed by Zehavi. Compared with the TCM encoder in (a), the BICM in (b) uses independent bit interleavers for all the bits of a symbol rather than a single symbol-based interleaver. The purpose of bit interleaving is:

- To disperse the bursty errors induced by the correlated fading and to maximize the diversity order of the system;
- To render the bits associated with a given transmitted symbol uncorrelated or independent of each other.

Since in BICM the bit-based minimum Hamming distance (the number of different bits between the erroneous path in the shortest error event and the correct path) is maximized, BICM will give a lower BER in Rayleigh fading channels than that of TCM that maximizes the FED. In other words, for the same complexity BICM achieves better code diversity (i.e., the minimum Hamming distance), while TCM achieves better minimum Euclidean distance. In fact, the three separate bit interleavers of size K can be replaced by a single bit-interleaver with size of $3K$, resulting in a generic BICM scheme as shown in Fig. 5.11.1 (c). In general, a BICM transmitter comprises an encoder for a binary code \mathcal{C} , a “bit interleaver,” and a signal mapper. The output sequence of the bit interleaver is segmented into m -bit blocks, which are mapped to a 2^m -point signal constellation using Gray coding. The BICM decoder implements the inverse process, as shown in Fig. 5.11.1 (c). Good performance close to capacity can be obtained if \mathcal{C} is a long Turbo code or LDPC code.

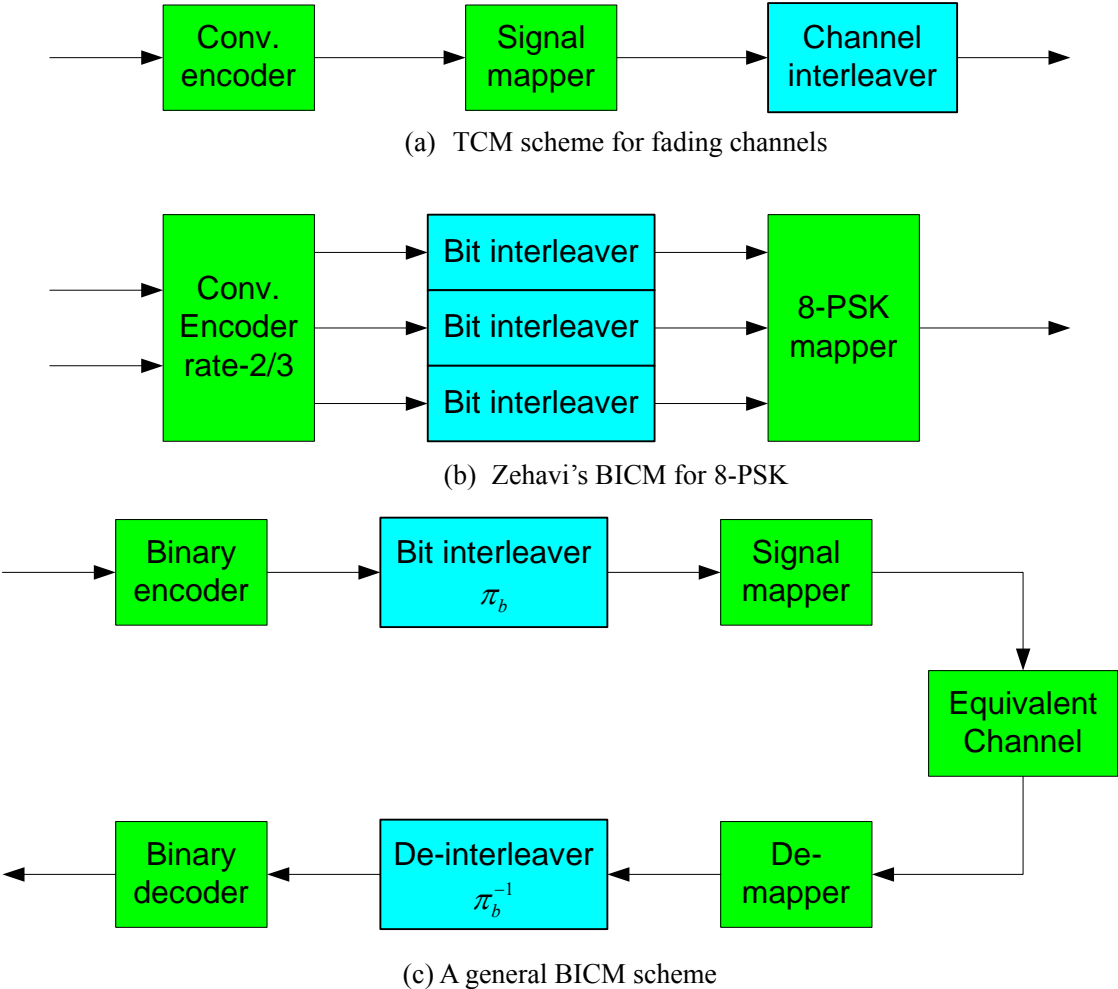


Figure 5.11.1

5.11.1 BICM-ID

BICM can be viewed as a special type of SCCC, and the “inner code” is the symbol

mapper, which can be considered as a nonrecursive single-state encoder. So the iterative decoding method for SCCC can be applied to BICM.

BICM with iterative decoding (BICM-ID) was proposed by Li and Ritcey [Li98] for further improving the FED of Zehavi's BICM scheme. This FED improvement can be achieved with the aid of combining SP(set partitioning)-based constellation labeling, as in TCM, and by invoking soft-decision feedback from the decoder's output to the demodulator's input, in order to exchange soft-decision based information between them.

The BICM-ID scheme using soft-decision feedback is shown in Fig. 5.11.2, where soft-in soft-out (SISO) detector/decoder is used in the receiver modulo. Let \mathcal{C} be a binary code. Assume that it is concatenated with an N -dim memoryless modulator over a signal set $\mathcal{X} \subseteq \mathbb{C}^N$ of size $|\mathcal{X}| = M = 2^m$, through a bit interleaver π and a one-to-one binary labeling map $f: \{0,1\}^m \rightarrow \mathcal{X}$. Denote the code sequence by \mathbf{c} . The interleaved sequence $\pi(\mathbf{c})$ is segmented into m -bit blocks denoted by $\mathbf{c}_t = (c_t^{(0)}, c_t^{(1)}, \dots, c_t^{(m-1)})$, which are mapped into signal points $x_t = f(\mathbf{c}_t)$ with \mathbf{c}_t as the label of x_t . The signal x_t are then transmitted over the channel at time t , resulting in the received signal y_t .

Let x denote a signal point in \mathcal{X} , and $b_i(x)$ the i th bit of the label of x . With the use of iterative demodulation/decoding at the receiver, the demapper can use the MAP algorithm to compute APPs for each label bit of x_t and deliver them to the decoder; i.e.,

$$P(c_t^{(i)} = b | y_t) = \sum_{x_t \in \mathcal{X}_b^{(i)}} P(x_t | y_t) \propto \sum_{x_t \in \mathcal{X}_b^{(i)}} p(y_t | x_t) P(x_t), \quad \text{for } i=1, \dots, m$$

where

$$\mathcal{X}_b^{(i)} = \{x \in \mathcal{X} | b_i(x) = b\} = \{x_t = f(\mathbf{c}_t) \in \mathcal{X} | c_t^{(i)} = b\}$$

is the subset of all the signals $x \in \mathcal{X}$ whose label has the value $b \in \{0,1\}$ in position i , and $P(x_t)$ is the *a priori* probability of transmitting x_t . At the first iteration, $P(x_t)$ is initialized to be $1/M$ for all values of x_t . 对于第二次及以后各次迭代,

$$P(x_t) = \prod_{j=0}^{m-1} P(c_t^{(j)} = b_j(x_t)) \quad (\text{with 充分长的交织器})$$

考虑到交织/解交织, 在图 5.11.2 中即为

$$P(x_t) = \prod_{j=0}^{m-1} P(v_t^{(j)} = b_j(x_t); I)$$

Therefore,

$$P(c_t^{(i)} = b | y_t) = \sum_{x_t \in \mathcal{X}_b^{(i)}} P(y_t | x_t) \prod_{j=0}^{m-1} P(c_t^{(j)} = b_j(x_t))$$

在迭代解调中，demapper 送给译码器的外信息为

$$P(c_t^{(i)} = b; O) = \frac{P(c_t^{(i)} = b | y_t)}{P(c_t^{(i)} = b; I)} = \sum_{x_t \in \mathcal{X}_b^{(i)}} \left(P(y_t | x_t) \prod_{\substack{j=0 \\ j \neq i}}^{m-1} P(c_t^{(j)} = b_j(x_t)) \right)$$

它被译码器看作输入的先验信息。在对数域中，它可以表示为

$$L_e^{demapper}(c_t^{(i)} = b) = \log P(c_t^{(i)} = b | y_t) - \log P(c_t^{(i)} = b; I)$$

The SISO decoder for FEC code is used for generating the APPs $P(u_t^{(i)}; O)$ of the information bits, as well as the extrinsic APPs $P(c_t^{(i)}; O)$ (应该是纯外信息，等于 $APP(c_t^{(i)} | y) / P(c_t^{(i)}; I)$ ，不包含信道值) of the coded bits, from the deinterleaved probabilities $P(v_t^{(i)} = b; O)$. It can be implemented based on the MAP, Max-Log- MAPA and other such algorithms.

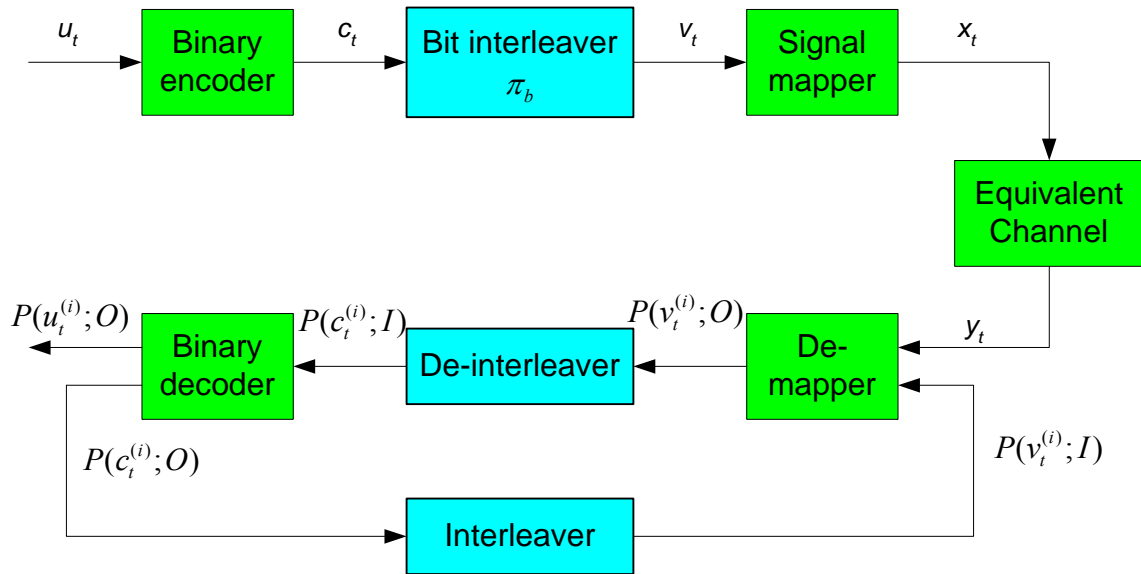


Figure 5.11.2. BICM-ID scheme using soft-decision feedback

■ Labeling method

It should be pointed that labeling plays a key role in BICM. The performance of BICM depends on the labeling used. Fig.x shows the process of subset partitioning for each of the three bit positions for both Gray labeling and SP labeling. It is seen that Gray labeling has a lower number of nearest neighbours compared to SP-based labeling. Hence, Gray labeling is a more appropriate mapping during the first decoding iteration, and so it is adopted by the non-iterative BICM scheme of Fig.x. With iterative decoding and SP-based labeling, BICM-ID can achieve a high diversity order as well as a high FED.

By using the density evolution approach for BICM, it is demonstrated that there is no one mapper having the best performance over all SNR regions [Tan05, IEEE Trans. Wireless, vol.4, no.2, 2005].

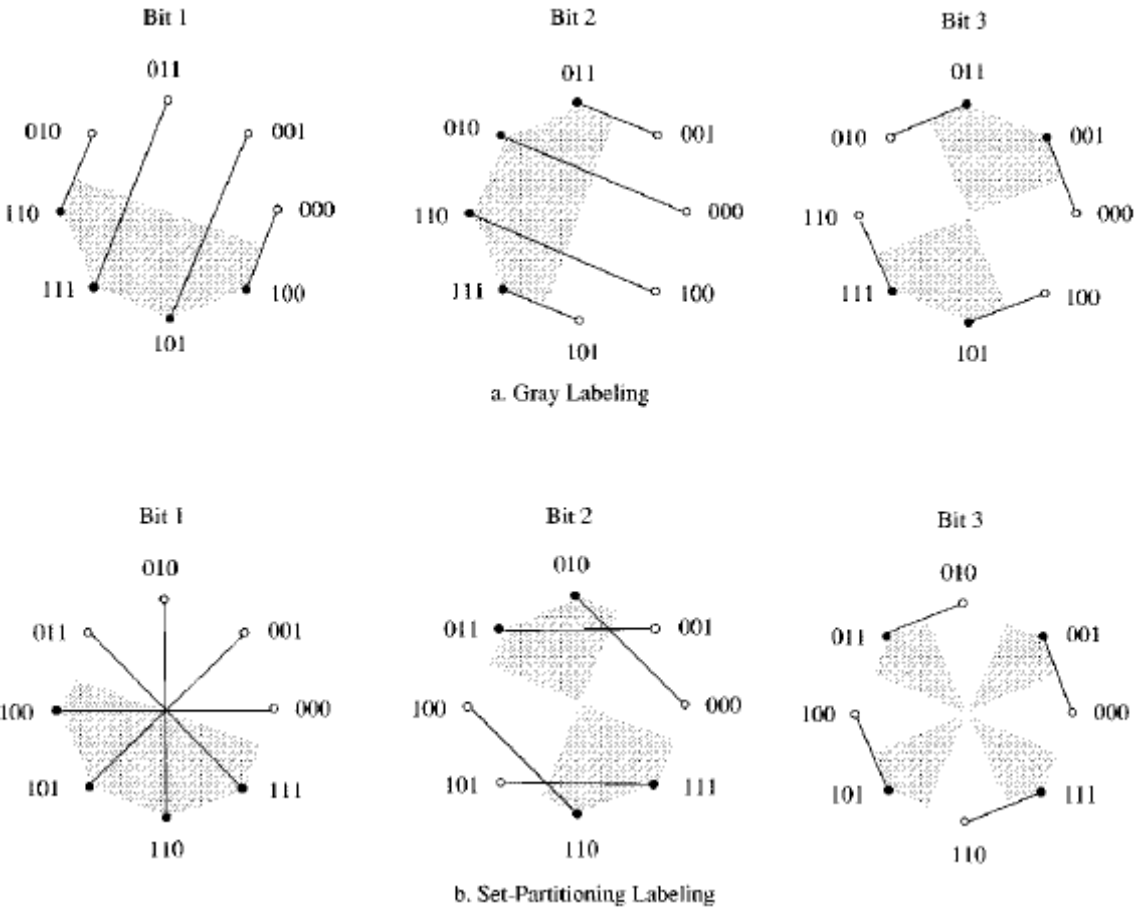


图 5.11.4 给出了 16-QAM 星座的 binary labeling rule.

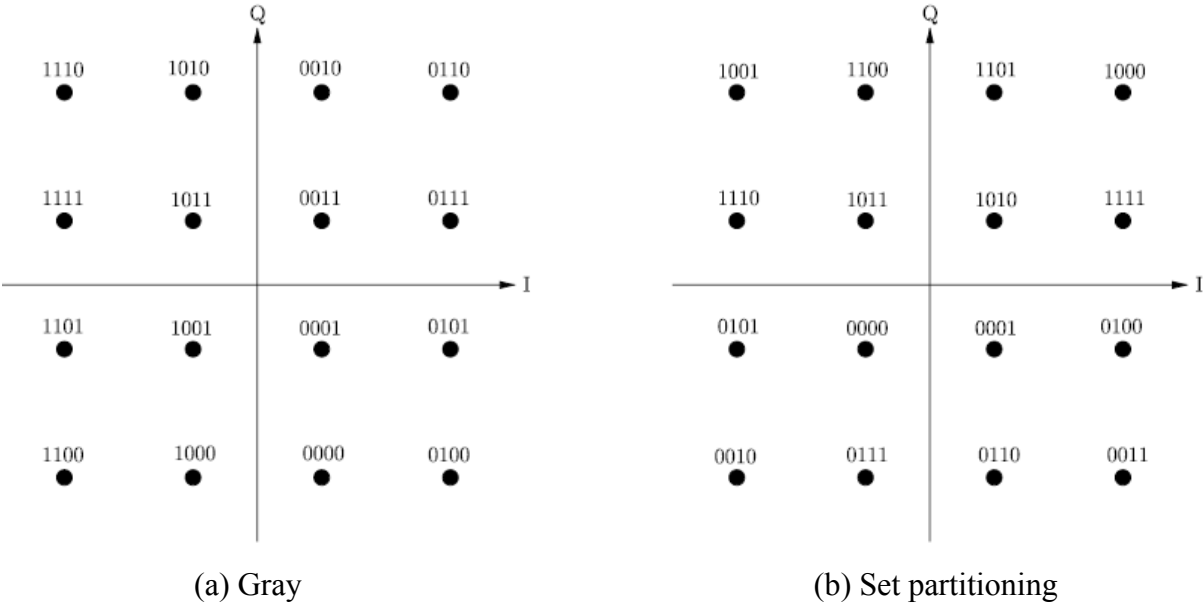


Figure 5.11.4 Binary labeling rules for 16-QAM

- Interleaver design: randomly generated.

5.11.2 More About BICM: Information-theoretic aspects [Gallager68, Caire98]

In Chapter 6 of [Gallager68], Gallager proved a coding theorem for parity-check codes, which may be addressed as follows.

- **Theorem:** Binary linear codes can be used to achieve capacity on an arbitrary discrete memoryless channel.

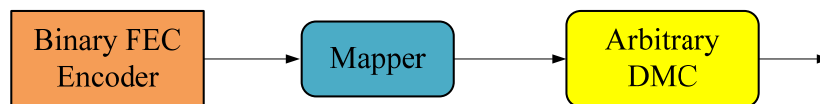


Figure 5.11.5

Gallager also demonstrated a simple algorithm to generate codewords with the probability distributions required to achieve the results of the coding theorem. However, the problem is that finding decoding algorithm is not simple.

Fig. 5.11.6 shows an example, where each channel codeword is a sequence of N ternary independent digits with the probabilities $Q(a)=3/8$, $Q(b)=3/8$ and $Q(c)=2/8$. We will call it Gallager mapping later.

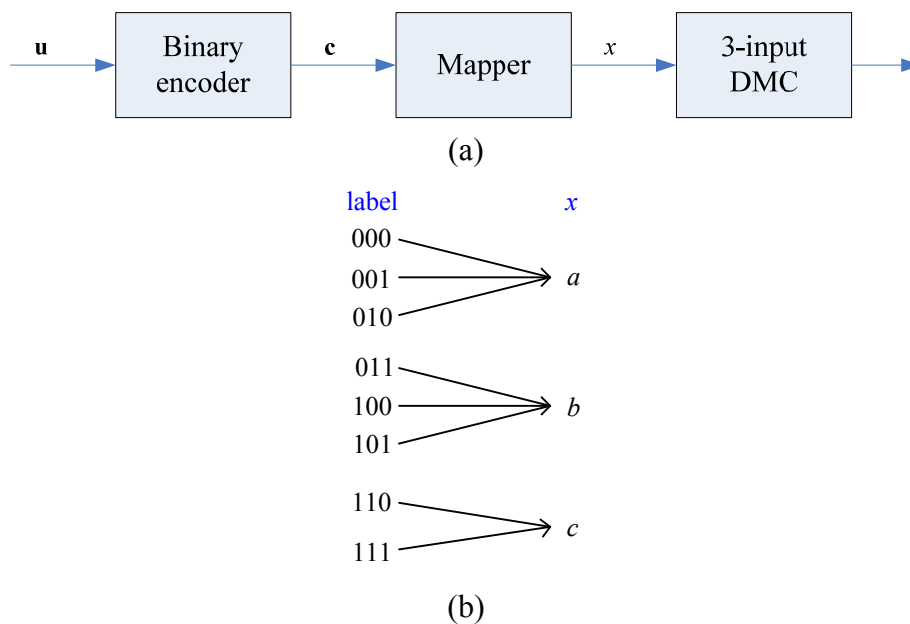


Figure 5.11.6 An example for use of binary codes on a DMC. (a) System model. (b) Mapping rule

Now, BICM-ID with the use of Turbo-like codes provides an effective solution. Joint demapping-decoding greatly reduces the decoding complexity.

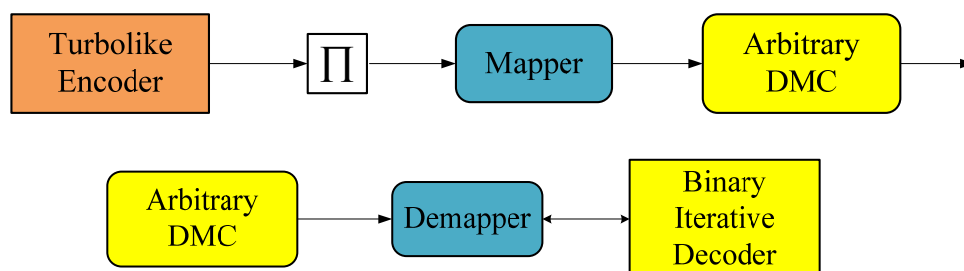


Figure 5.11.7

Caire *et al.* provided in [IT1998] a comprehensive analysis of BICM in terms of information rates and error probability, showing that in fact the loss incurred by the BICM interface may be very small. Furthermore, this loss can essentially be recovered by using iterative decoding.

Coded-modulation capacity for various signal constellation in the AWGN channel has been discussed in Chapter 2. Here, we briefly review the results on the achievable rates for BICM by following Caire.

Define the sets

$$\mathcal{X}_{b_{i_1}, \dots, b_{i_l}}^{(i_{j_1} \dots i_{j_l})} = \left\{ x \in \mathcal{X} \mid b_{i_{j_1}}(x) = b_{j_1}, \dots, b_{i_{j_l}}(x) = b_{j_l} \right\}$$

as the subsets of signal points having the l binary labels b_{j_1}, \dots, b_{j_l} in positions $i_{j_1} \dots i_{j_l}$.

Under the assumption of an infinite-length interleaver, capacity and cutoff rate were studied in [Caire98]. This assumption yields a set of m independent parallel binary-input channels, for which the corresponding mutual information is the sum of the corresponding rates of each subchannel, and are given by

$$\begin{aligned} I^{\text{ind}}(X; Y) &= \sum_{i=1}^m \mathbb{E} \left[\log \frac{\sum_{x' \in \mathcal{X}_B^i} P_{Y|X}(Y | x')}{\frac{1}{2} \sum_{x' \in \mathcal{X}} P_{Y|X}(Y | x')} \right] \\ &= m - \sum_{i=1}^m \mathbb{E}_{B, Y} \left[\log \frac{\sum_{x' \in \mathcal{X}} P_{Y|X}(Y | x')}{\sum_{x' \in \mathcal{X}_B^i} P_{Y|X}(Y | x')} \right] \end{aligned}$$

where B is a random variables taking values on $\{0, 1\}$. The joint distribution $p(B, Y)$ of the channel- i is

$$p(B, Y | i) = 2^{-m} \sum_{x \in \mathcal{X}_B^i} p_{Y|X}(y | x)$$

The BICM capacity is given by

$$C^{\text{BICM}} \equiv I^{\text{ind}}(X; Y)$$

Since BICM can be regarded as MLC with (Gray mapping and) parallel independent decoding (i.e., decoder at level i makes no use of decisions of other levels $j \neq i$), it is shown that [Wachsmann-Huber99]

$$C^{\text{BICM}} = \sum_{i=1}^m \frac{1}{2} \sum_{b=0}^1 \left(C_{\mathcal{X}}^{\text{CM}} - C_{\mathcal{X}_B^{(i)}}^{\text{CM}} \right)$$

where $C_{\mathcal{A}}^{\text{CM}}$ is the capacity (information rate) for coded modulation over a general constellation \mathcal{A} .

The BICM (或MLC/PDL) approach is simply a suboptimum approximation of an

optimum coded modulation scheme, its capacity strongly depends on the particular labeling of signal points. Caire *et al.* showed that the gap to an optimum scheme is surprisingly small with Gray labeling of the signal points. However, it has been illustrated that the gap increases significantly if the finite length of the code is taken into account. 码长越短, 性能差别越大。

Figure 5.11.8 shows the BICM mutual information for some signal constellations, different binary labeling rules and uniform inputs for the AWGN channel, as a function of SNR. For illustration simplicity, we have only plotted the information rate for the Gray and set partitioning binary labeling rules from Figure x. Observe that binary reflected Gray labeling pays a negligible penalty in information rate, being close to the coded modulation capacity.

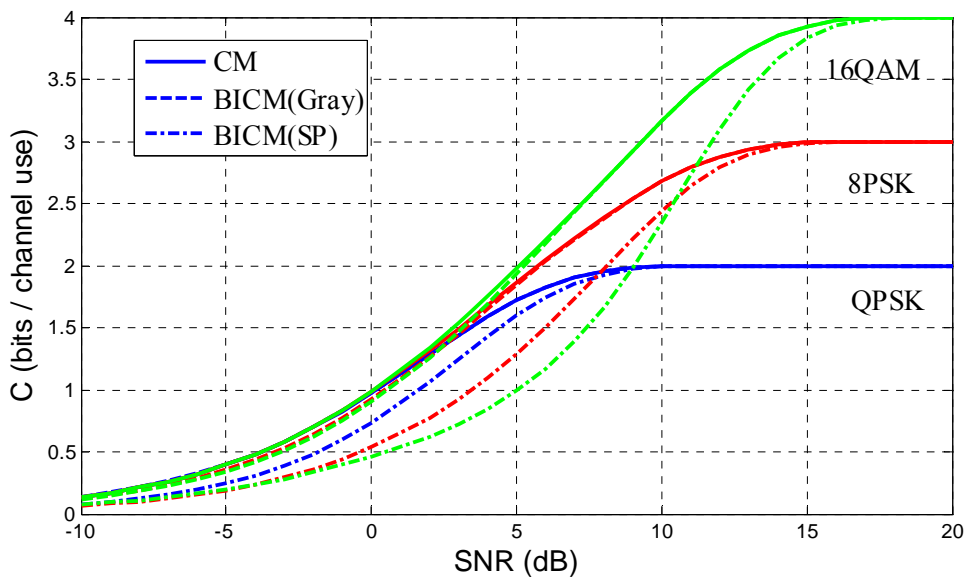


Fig. 5.11.8 Coded modulation and BICM capacities (in bits per channel use) for multiple signal constellations with uniform inputs in the AWGN channel. Gray and set partitioning labeling rules correspond to dashed and dash-dotted lines, respectively. The thick solid lines indicate CM channel capacity.

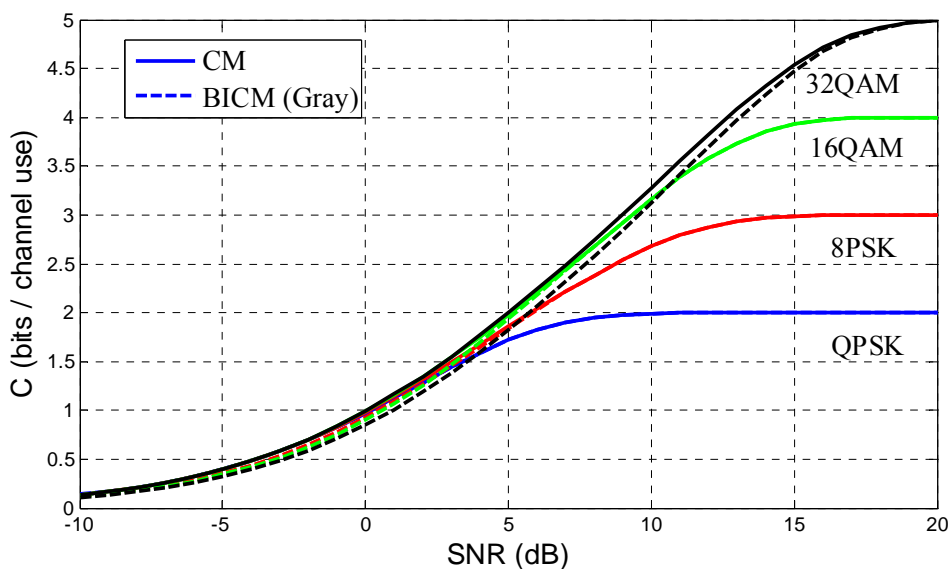


Fig. 5.11.9

Comparison with Multilevel Coding:

While MLC with MSD achieves the coded modulation capacity, it does not achieve the coded modulation error exponent. This is due to the MLC (with or without MSD) error exponent always being given by the minimum of the error exponents of the various levels, which results in an error exponent smaller than 1. While BICM suffers from a nonzero, yet small, capacity loss compared to CM and MLC/MSD, BICM attains a larger error exponent, whose loss with respect to CM is small. This loss may be large for an MLC construction. In general, the decoding complexity of BICM is larger than that of MLC/MSD, since the codes of MLC are shorter. One such example is a code where only a few bits out of the m are coded while the rest are left uncoded. In practice, however, if the decoding complexity grows linearly with the number of bits in a codeword, e.g., with LDPC or turbo codes, the overall complexity of BICM becomes comparable to that of MLC/MSD.

Summary: Since its introduction, BICM has been regarded as a pragmatic yet powerful scheme to achieve high data rates with general signal constellations. Nowadays, BICM is employed in a wide range of practical communication systems, such as DVB-S2, Wireless LANs, DSL, WiMax, and the 4G cellular systems.

5.12 Q-ary LDPC-coded Modulations

5.13 Combined Coding and Shaping

从图 5.1.7 可知, 采用均匀的 2D 信号集, 最好的系统性能最多只能达到 constrained-capacity, 而此极限距离 Shannon 容量限还有 1dB 左右的差距。To achieve the Shannon-capacity-approaching performance (in the high SNR regime) for coded-modulation systems, it is necessary to use constellation shaping in conjunction with coding. Modern channel coding techniques are subjects of the previous chapters, and the related shaping methods are discussed below.

5.13.1 Overview of Constellation Shaping Methods

从前面关于成形增益的讨论中, 我们知道信号星座成形基本上有两种技术:

- 第一种我们称为 *几何成形*, 使信号星座的几何形状类似于球体(在高维信号空间中);
- 第二种我们称为 *概率成形*, 使发送的信号具有与正态分布相近的分布。

在编码调制系统中具体实现时, 这两种成形技术可以有多种实现方法, 但大体上可以分为两大类: 单层编码与两层编码方法。

在两层方案中[Forney84], 一层为信道编码, 另一层为信源编码(成形编码)。图 5.13.1 所示是编码与成形结合的两层方案。首先把一个给定的 n -维信号星座 \mathcal{A} 划分成若干个信号点子集 $\mathcal{A}_i, 1 \leq i \leq m$ 。二进制数据流 \underline{u} 按照一定的速率划分为两个子数据流 $\underline{u}^{(c)}$ 和 $\underline{u}^{(s)}$ 。子数据流 $\underline{u}^{(c)}$ 进入一个信道编码器, 输出的序列 $\underline{c}=(c_1, \dots, c_j, \dots, c_L)$ 用来选择信号子集序列 $\underline{s}=(s_1, \dots, s_i, \dots, s_N)$, 其中 $s_i \in \{\mathcal{A}_i, 1 \leq i \leq m\}$ 。这一层称为信道编码层。子数据流 $\underline{u}^{(s)}$ 进入一个成形编码器, 输出的序列用来选择一个特定的信号点序列 $\underline{x}=(x_1, \dots, x_i, \dots, x_N)$, 其中 x_i

是子集 s_i 里的信号点。这一层称为信源编码层。根据不同的信号选择方法，信号星座中每个点的使用概率或许不一样。

信道编码层的作用是在子集序列中引入冗余，从而使得接收端能够无误地（以尽可能小的错误概率）恢复子集序列。信源编码层的作用是针对给定的速率，选择信号点使得信号星座的平均能量尽可能小；等价地，对于给定的平均能量，选择尽可能多的信号点使得传输速率尽可能高。

两层方案的最佳性（从达到信道容量的角度）是基于编码和成形的可分性的。已经证明，对于高信噪比的系统，如果信道编码层和信源编码层分开设计并适当地构成一个两层系统，则信道容量的损失是可以忽略的[Forney2000]。

图 5.13.2 所示是编码和成形结合的单层方案。二进制数据序列 \underline{u} 进入信道编码器，产生输出码字 \underline{c} 。码字 \underline{c} 进入成形映射器后输出信号序列 \underline{x} 。在该方案中，信号映射器具有成形编码功能，它把均匀等概的二进制序列转化为统计特性与信道特性相匹配的信道符号序列，使得相应的互信息尽可能地大。在此基础上，再设计一个（二元或多元）信道码，以逼近这个互信息，从而逼近信道容量。单层结构的最佳性是由 Gallager 引理保证的[Gallager68]，其对所有的信噪比都成立。理论上，在接收端可以实现最小误比特率(BER)译码 / 解映射算法。在实际中，可以采用迭代的译码 / 解映射算法。这时，往往要在编码器和映射器之间引入一个随机交织器。

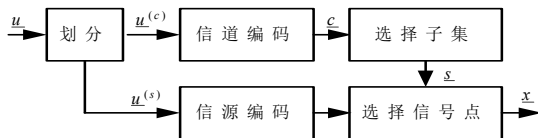


图 5.13.1 编码与成形结合的两层实现方案。

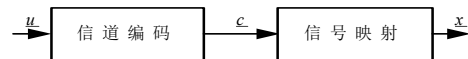


图 5.13.2 编码与成形结合的单层实现方案。

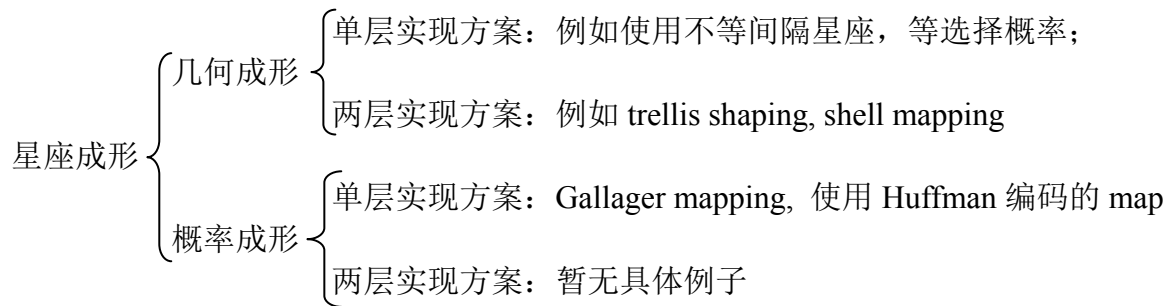
如果允许使用变速率的成形编码，则一个简单的方法是使用前缀码（如 Huffman 编码）。这种方法可以认为是**概率成形**方法，其出发点是计算最佳的信源分布，然后利用不等长的编码技术去逼近这个分布。可以证明，对于给定的平均能量，使得速率最大的分布是 Maxwell-Boltzmann 分布^[4]。若以此为“信源分布”，则前缀码是最佳的。Livingston 把低维的信号星座划分成几个大小不等的子星座，然后利用不等长编码获得成形增益，可以认为是**几何成形**方法。变速率编码的优点是其考虑的信号点都来自低维信号星座，因而映射/解映射（无论用算法还是用查表）容易实现。但是，正如 Forney 指出的那样，变速率成形的最大问题是数据需要缓存和再同步，因而限制了其实用范围。

固定速率编码的目的是使得信号星座的形状接近于球体。但是，要逼近信道容量，信号星座的维数必须足够大。Forney（针对两层方案）提出了一种基于无限维空间的成形技术——“篱笆图成形” (Trellis Shaping)，可以很容易地获得 1dB 左右的成形增益。还有一种实用的技术是“壳映射” (Shell Mapping) [9]，这些可以看作是**几何成形**方法，在维数适中的情况下可以获得部分成形增益。

在单层方案中，使用不等星座点间隔的信号星座（如 Sun 和 van Tilborg 提出的不等间隔的 PAM 信号星座，一个例子见下图），可以看作是**几何成形**方法。Gallager 提出的多对一映射[Gallager68]、X. Ma 和 Li Ping 提出的线性叠加映射[Ma04]，均使得信号的信号点概率分布接近于正态分布，从而获得成形增益，它们属于**概率成形**方法。



小结：综上所述，我们可以将信号星座成形方法总结如下：



下面我们着重讨论两层方案中的几何成形与单层方案中的概率成形。二者的联系在于，高维球体（或类球体）在任一维上的投影近似服从正态分布。二者的区别在于，前者依靠优化高维信号星座的形状来获得成形增益，而后者依靠优化低维信号的概率分布来获得成形增益。前者在译码时一般不需要译码器和映射器之间进行迭代，而后者通常需要实现迭代的译码-解映射算法。

5.13.2 Gallager Mapping

令 X 表示信道的输入符号， Y 表示信道的输出符号。对于一个给定的信号星座 \mathcal{A}_x ，假定 $P_x^*(x), x \in \mathcal{A}_x$ 是信道的最佳输入分布（能使互信息 $I(X;Y)$ 最大化）。Gallager 映射器的基本设计方法如下：

首先将信道编码器输出的编码比特序列 \mathbf{c} 按一定长度进行分组 $\mathbf{v}_0, \mathbf{v}_1, \mathbf{v}_2, \dots$ ，然后采用多对一的映射方法，将一个或多个比特序列 \mathbf{v}_i 映射到 \mathcal{A}_x 的每一个星座点上，使得由此导致的星座点选择概率（即 X 的实际分布）近可能接近于 $P_x^*(x)$ 。

图5.13.4是一个使用4-PAM星座时的Gallager映射例子。在接收端，我们需要采用BICM-ID这种软信息迭代联合解调/译码方式来进行信号检测。

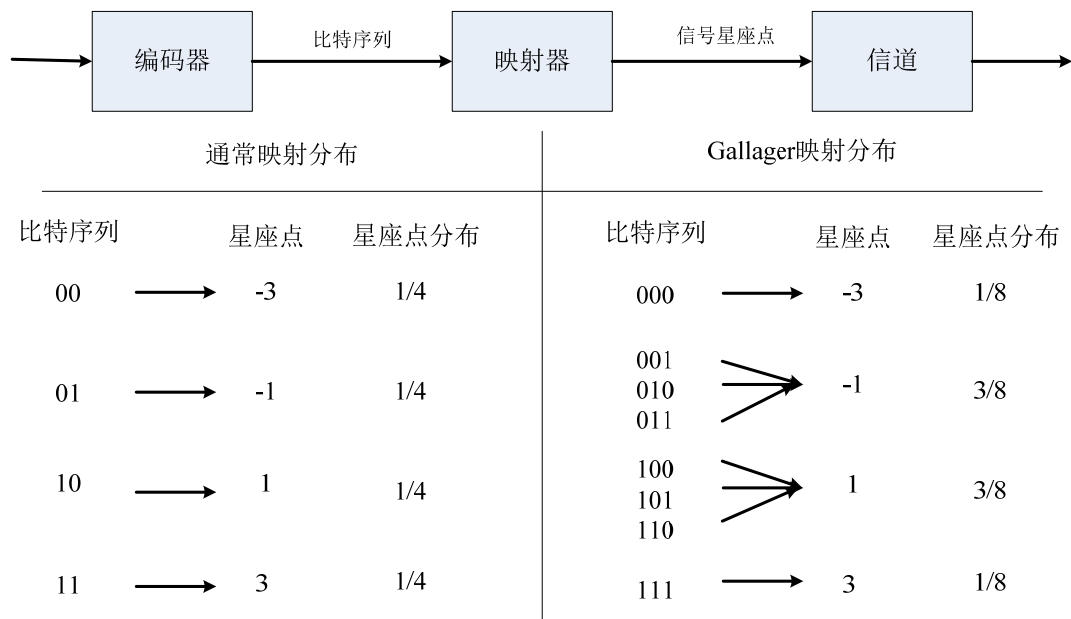


图 5.13.4

类似于BICM，对于有限码长，在Gallager映射器中采用不同的labeling策略，系统的BER性能也会不同。对于BICM系统中Gallager映射器的优化设计，我们提出采用下述的labeling设计准则：

- 1) 对于同一组内的不同标号 (label)，设计的时候尽量最小化标号之间的最大汉明距离；
- 2) 对于不同组内的不同标号，设计的时候同样尽量最小化标号之间的最大汉明距离。

Example 5.13.1 将4比特长符号调制到8-PAM星座的Gallager映射

	-7	-5	-3	-1	1	3	5	7
准则1+2+3			1001	1101	0101	0010		
	1100	1000	1010	1110	0110	0011	0000	0100
			1011	1111	0111	0001		

图 5.13.5

该映射不但考虑了星座点使用概率近似离散高斯分布，而且最小化了组内以及组外相邻标号之间的最大汉明距离。经过这样的优化设计，不但给系统带来了成形增益，而且在解调译码出错的时候，最大程度地降低了系统的误比特率。

对于PAM 信号的设计可以直接推广至常用的QAM 调制。下面给出一个将符号长度为5比特的符号映射到16-QAM星座图上的Gallager 映射器具体图样。

Example 5.13.2 将5比特长符号调制到16-QAM星座的Gallager映射

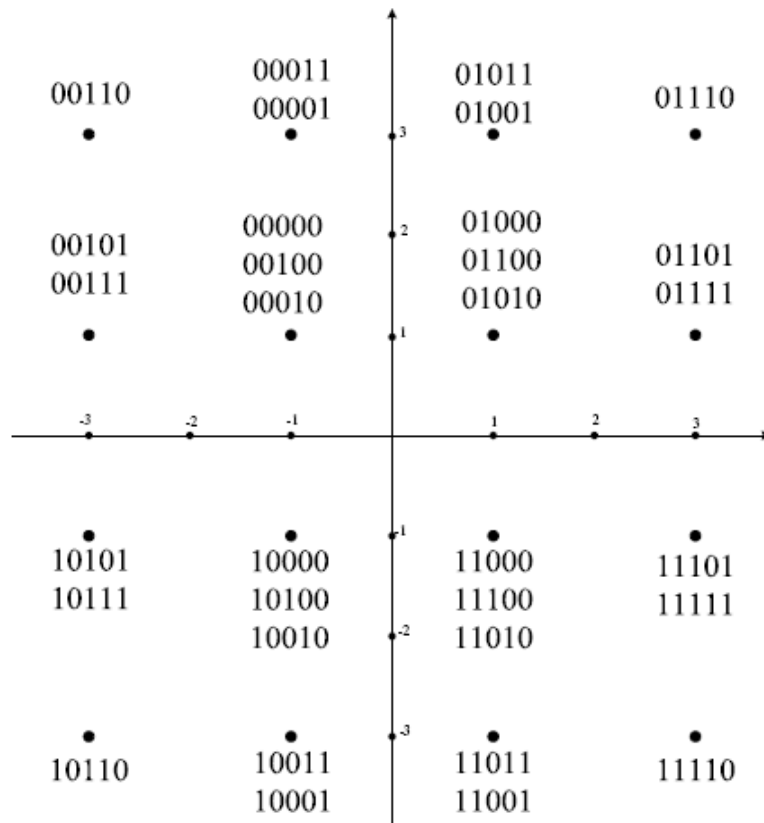
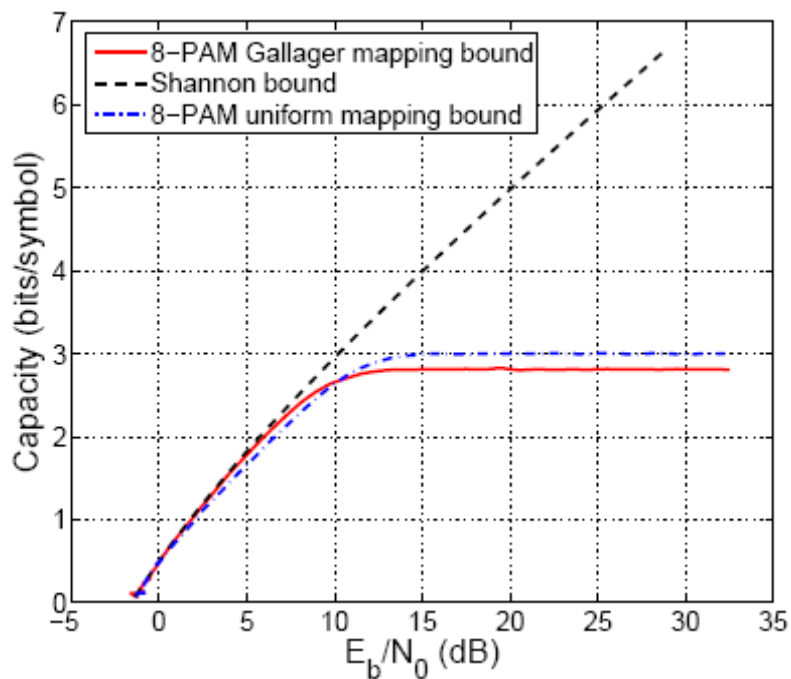
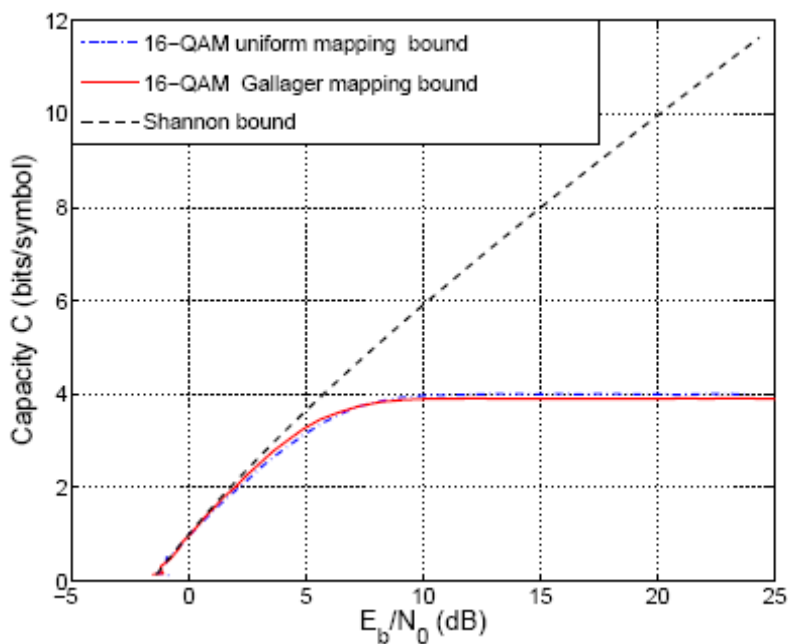


图 5.13.6

在上述 Gallager 映射器所给出的输入分布下,采用 8-PAM 与 16-QAM 星座的编码调制系统的信道容量分别如图 5.13.7(a)和(b)所示。



(a) 8-PAM



(b) 16-QAM

图 5.13.7 不等概输入分布下编码调制系统的容量

下面我们以基于LDPC码的BICM-ID系统为例，来讨论有限码长下采用Gallager映射器的具体性能。LDPC码选取了中国移动多媒体广播(China Mobile Multimedia Broadcasting, CMMB)标准中的1/2码率规则二元LDPC码，该码校验矩阵的行重为6，列重为3，码长为9216比特。信号映射器采用图5.13.6所示的16-QAM Gallager映射器，假设信道模型为AWGN。LDPC码译码器采用和积算法(SPA)，最大译码迭代次数设定为10次；而解映射器与译码器之间的外部迭代次数设定为5次。图5.13.8显示了各种不同设计

准则下谱效率为2.5 bits/s/Hz的Gallager映射编码调制系统仿真结果。可以观察到，当BER=10⁻⁵时，优化的映射设计方案比未优化的自然映射方案获得的增益超过1dB；与相同谱效率的常规均匀32-QAM调制对比，优化后的Gallager映射系统BER性能大约要好0.25 dB。

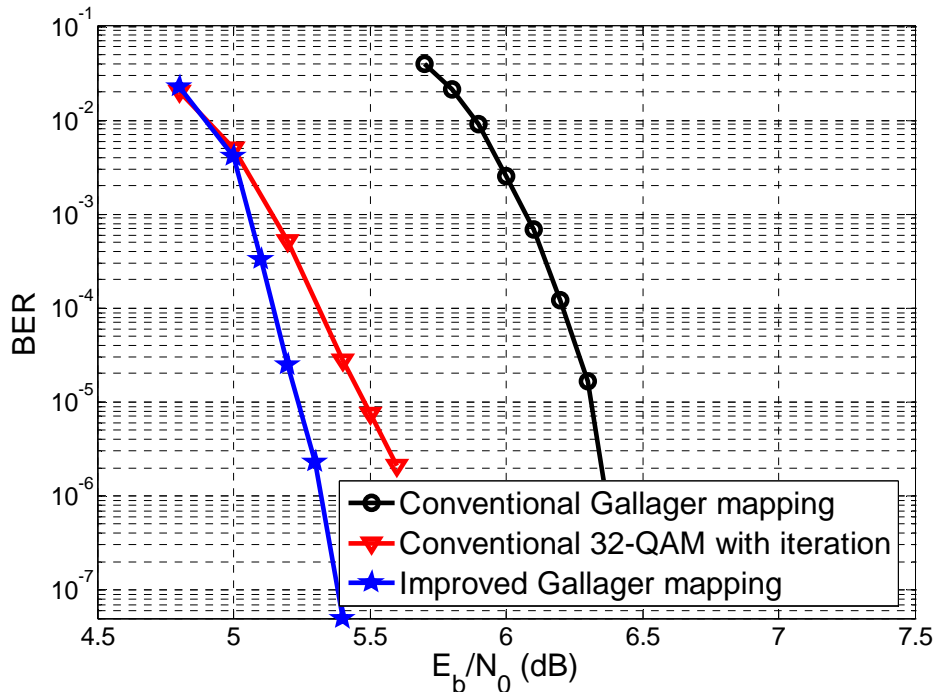


图 5.13.8

EXIT Chart分析:

下面我们以EXIT chart 作为分析工具，从理论的角度来分析前述的Gallager映射器设计准则的有效性。EXIT chart 性能分析原理框图如图5.13.9所示。

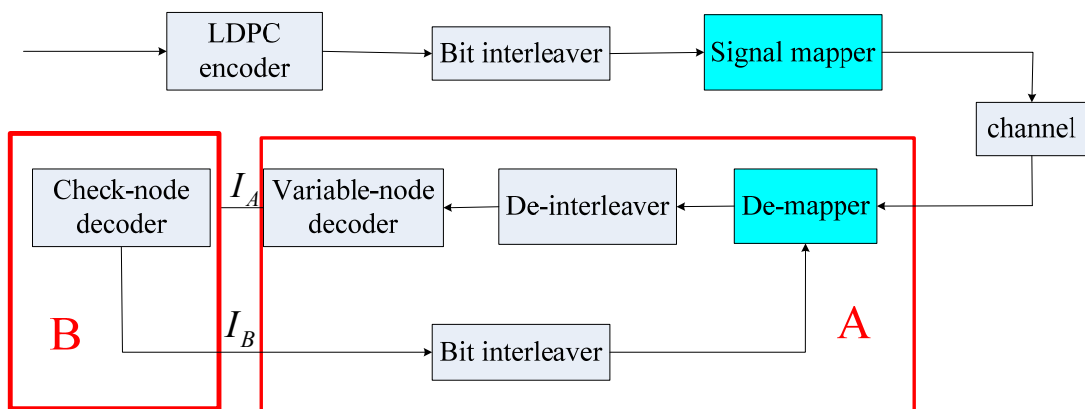


图5.13.9

在图5.13.9中，模块A包括DeM以及VND，而模块B只包括CND 一部分。模块A输出的互信息记为I_A，模块B输出的互信息记为I_B，DeM 输出的互信息记为I_D。模块A的因子图如图5.13.10所示。

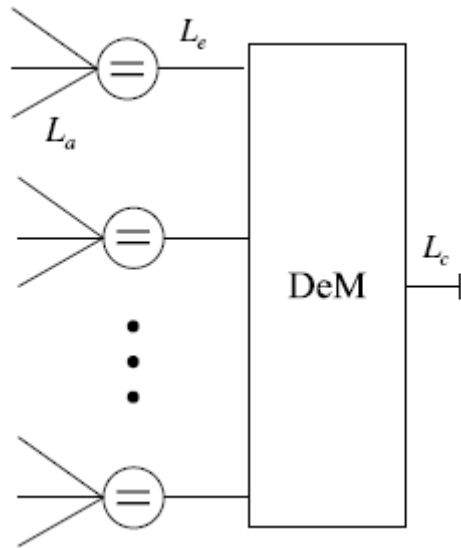


图5.13.10 模块A的Forney 型因子图

应用对LDPC码进行EXIT Chart分析的类似方法，我们可以画出满足不同映射准则的EXIT曲线，图5.13.11给出了8-PAM Gallager映射器的分析结果。其中LDPC码集合为规则LDPC码集合 $\mathcal{C}(3, 6)$ 。

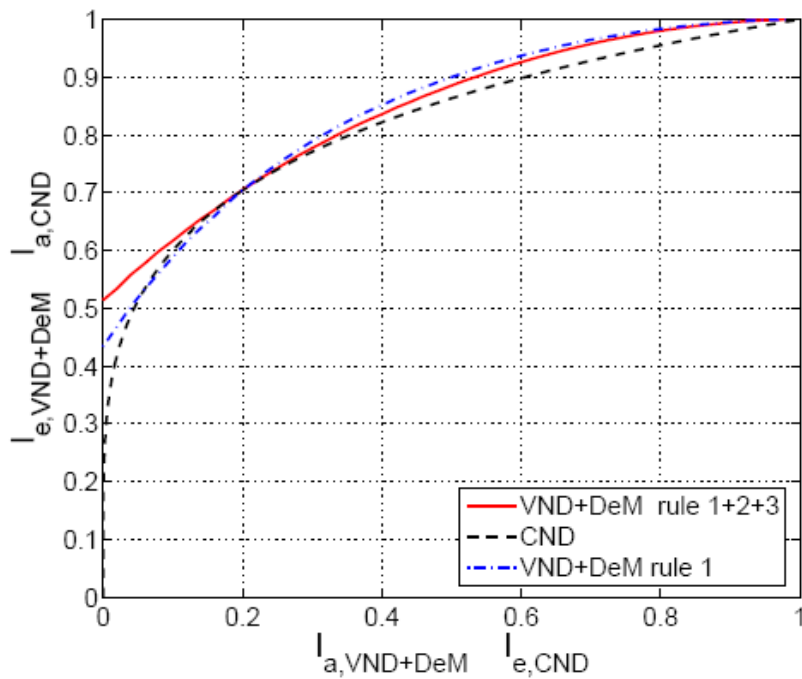


图5.13.11 8-PAM Gallager映射EXIT chart 分析@ $E_b=N_0=7.9$ dB

5.13.3 叠加 Mapping

将经单层或多层信道编码后的数据流划分为多层（如 K 层）比特流，记第 k 层中的

二进制比特流为 $\underline{v}^k = (v_1^k, \dots, v_N^k)$ 。在 t 时刻，所有 K 层的编码符号 v_t^k 组成一个矢量 $\underline{v}_t = (v_t^0, v_t^1, \dots, v_t^{K-1})$ ，经过信号映射器映射到信号集 A 中的一个信号点 $x_t \in A$ 。线性叠加映射器的结构如图 5.13.6 所示。

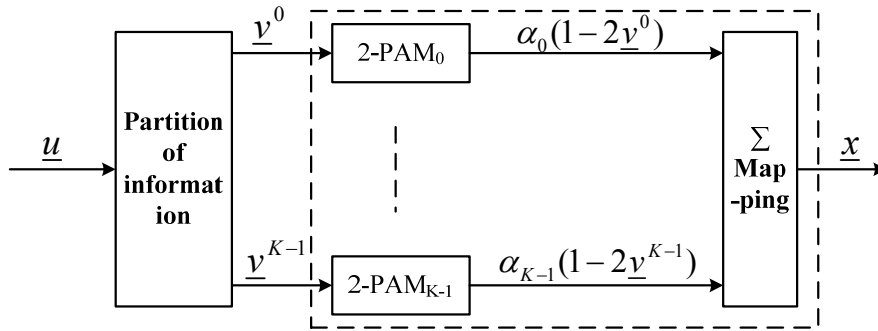


图 5.13.6 叠加映射器结构

在具体映射过程中，各层编码符号首先被 2-PAM 映射器映射成数据流 $\alpha_k \cdot (1 - 2v^k)$ ， $k \in \{0, 1, \dots, K-1\}$ ，其中 α_k^2 是第 k 层信息所对应的能量。然后， Σ 映射器将所有 K 层信号进行求和，形成一种“和”信号 x ：

$$\underline{x} = \sum_{k=0}^{K-1} \alpha_k \cdot (1 - 2v^k)$$

这里， $\{\alpha_k\}$ 满足 $\sum_{k=0}^{K-1} \alpha_k^2 = E_s$ 。如果所有 α_k 相同，则映射器称为 type-I sigma-mapper；否则，

称为 type-II sigma-mapper。由 type-I sigma-mapper 产生的信号星座是等间隔、不等概率的，如图 5.13.7 所示。由 type-II sigma-mapper 产生的信号星座一般是不等间隔的。

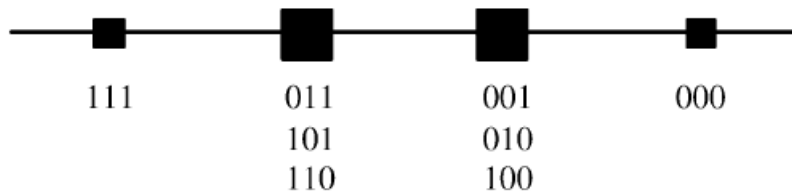


图 5.13.7 一个 sigma mapping with $K=3$ 的例子。In this case, $P_x = \{1/8, 3/8, 3/8, 1/8\}$. 对应信号集为 $A = \{-3, -1, 1, 3\}$ with $\alpha_0 = \alpha_1 = \alpha_2 = 1$ 。

在 type-I sigma-mapper 中，各层对应的信号能量相同，采用互信息设计准则，各层具有不同的码率，这样就类似于前述的 Multilevel coding 方案。在 type-II sigma-mapper 中，所有层可采用码率相同的信道码，但是每一层对应不同的能量；通过适当调节层间的能量关系，可达到在接收端各层能正确译码。功率分配方案有多种形式，可参考文献[?]。

当各层的信道码相同（包括码率）时，一种最简单的功率分配方案如下：设 t 时刻发送信号总能量为 E_s ，则各层信号能量 α_k^2 之间的约束关系为

$$\begin{cases} \sum_{k=0}^{K-1} \alpha_k^2 = E_s \\ \alpha_k^2 / \left(1 + \sum_{j>k} \alpha_j^2\right) = \alpha_{k-1}^2, \quad k = K-2, K-3, \dots, 0 \end{cases} \quad (11)$$

这里我们对信道噪声方差进行了归一化处理，即 $\sigma_n^2 = 1$ 。

在传统的多层编码调制系统中，互信息的链式法则表现为系统中各层之间的速率分配，而这里表现为各层之间的功率分配。

In [Ma-Li04], 一种基于叠加映射的多层编码调制方案 is proposed.

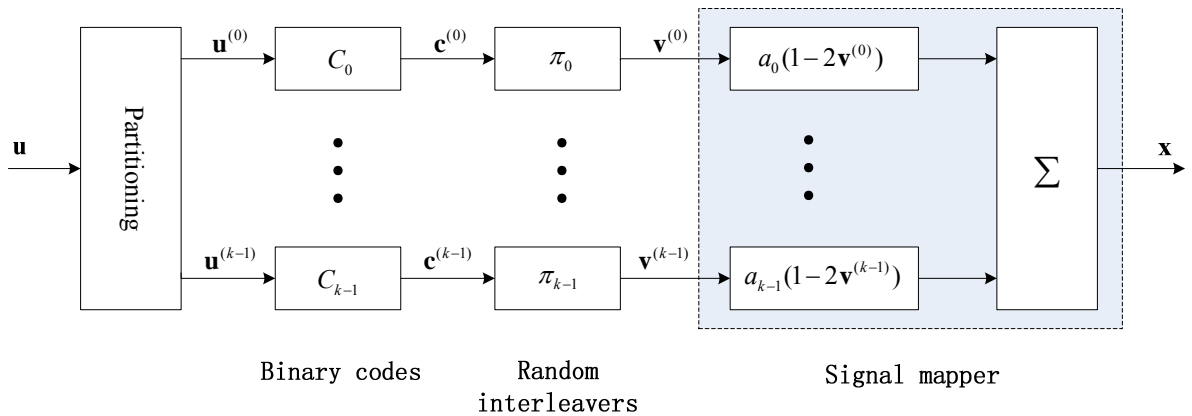
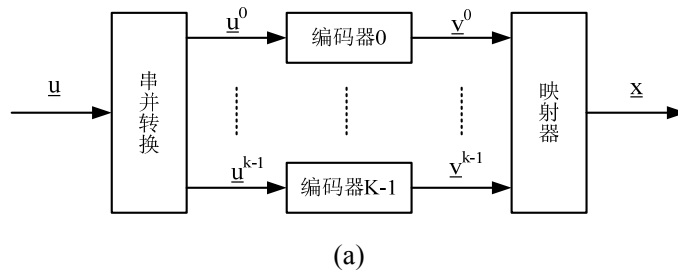


图 5.13.8

类似于对多址信道接收信号的处理，对于接收到的叠加编码信号，接收端可采用 successive interference cancellation (SIC)或高斯近似方法进行解映射与译码。

下面以第 k 层为例，说明高斯近似解映射算法。假定各层采用 LDPC 编码，其译码结构框图如图 5.13.8 所示。信道接收到的信息 \mathbf{y} 和其它层的软输出外信息 $\Lambda_{j/k}$ 一起输入解映射器，通过高斯近似解映射算法，得到分量码译码器的软输入信息 L_{in}^k 。



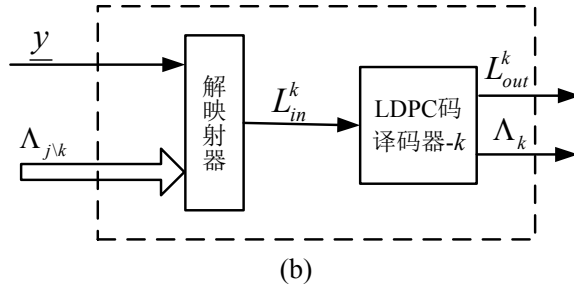


图 5.13.8 第 k 层译码器框图

高斯近似解映射算法如下：

设信道噪声、接收端的接收信号以及第 k 层的编码输出信号分别表示为随机变量 W 、 Y 和 V^k ，则有：

$$Y = \sum_{k=0}^{K-1} \alpha_k (1 - 2V^k) + W \quad (12)$$

现在考虑对信号 V^k 进行解映射，则(12)式可以改写为

$$Y = \alpha_k (1 - 2V^k) + \tilde{W} \quad (13)$$

其中 $\tilde{W} = W + \sum_{i \neq k} \alpha_i (1 - 2V^i)$ 。不失一般性，我们总假设信道噪声的方差 $\sigma^2 = 1$ ；而且将其它各层信息以及信道噪声一起近似看成是一种高斯噪声，即 \tilde{W} 近似看作满足高斯分布

$\tilde{W} \sim N(\mu_{\tilde{W}}, \sigma_{\tilde{W}}^2)$ ，其中

$$\mu_{\tilde{W}} = \sum_{i \neq k} \alpha_i (1 - 2\mu_{V^i}), \quad \sigma_{\tilde{W}}^2 = 1 + \sum_{i \neq k} 4\alpha_i^2 \sigma_{V^i}^2$$

$$\mu_{V^i} = P_{V^i}^{(a)}(1), \quad \sigma_{V^i}^2 = P_{V^i}^{(a)}(0)P_{V^i}^{(a)}(1)$$

则有

$$P_{V^k}^{(e)}(m) \propto \exp\left(-\frac{(y - \alpha_k(1 - 2m) - \mu_{\tilde{W}})^2}{2\sigma_{\tilde{W}}^2}\right) \quad (14)$$

其中 m 取值为 0 或 1。根据(14)式可知，在对数域中，第 k 层译码的软输入信息可表示为：

$$L_{in}^k = \frac{2\alpha_k(y - \mu_{\tilde{W}})}{\sigma_{\tilde{W}}^2} \quad (15)$$

5.13.4 Trellis Shaping

5.14 Implementation Considerations and Application Examples

Coded-modulations have been widely used in various modern communication systems, including voice modems as typical examples for TCM applications. Other applications include mobile communications, DVB, digital TV, and etc.

5.14.1 Multidimensional TCM Example: The V.34 Modem Standard

(V.34, V.92, Pragmatic TCM)

In this subsection, we discuss the TCM scheme used for the V.34 voice-band modem standard. This modem is capable of transmitting up to 33.6 kbps over the standard telephone system. Some of the aspects related to the error correction coding are summarized as follows [Forney96].

- The modem is adaptive in the symbol rate it employs and the size of the constellation. It is capable of sending at symbol rates of 2400, 2743, 2800, 3000, 3200, or 3429 symbols/second. (These peculiar-looking choices are rational multiples of the basic rate of 2400 symbols/second.) The symbol rate is selected by a line probing sequence employed during initialization which determines the available bandwidth.
- The modem is capable of transmitting variable numbers of bits per symbol. At the highest rate, 8.4 bits/symbols are carried. Rate is established at link initialization, and rate adjustments can occur during data transmission.
- Adaptive precoding and decision feedback equalization is also employed to compensate for channel dispersion.
- Shaping via shell mapping is employed, which provides modest gains in addition to the coding gains.
- Adaptive trellis coding is employed. The main code is a 16-state four-dimensional trellis code. This code provides 4.66 dB of gain and is rotationally invariant. However, two other trellis codes are also included: a 32-state four-dimensional code with 4.5 dB of gain and a 64-state four dimensional code providing 4.7 dB of gain.

V.34 modem的编码调制系统框图如图5.14.1所示。The trellis encoder for the modem is shown in Figure 5.14.2, with the corresponding convolutional encoder in Figure 5.14.3.

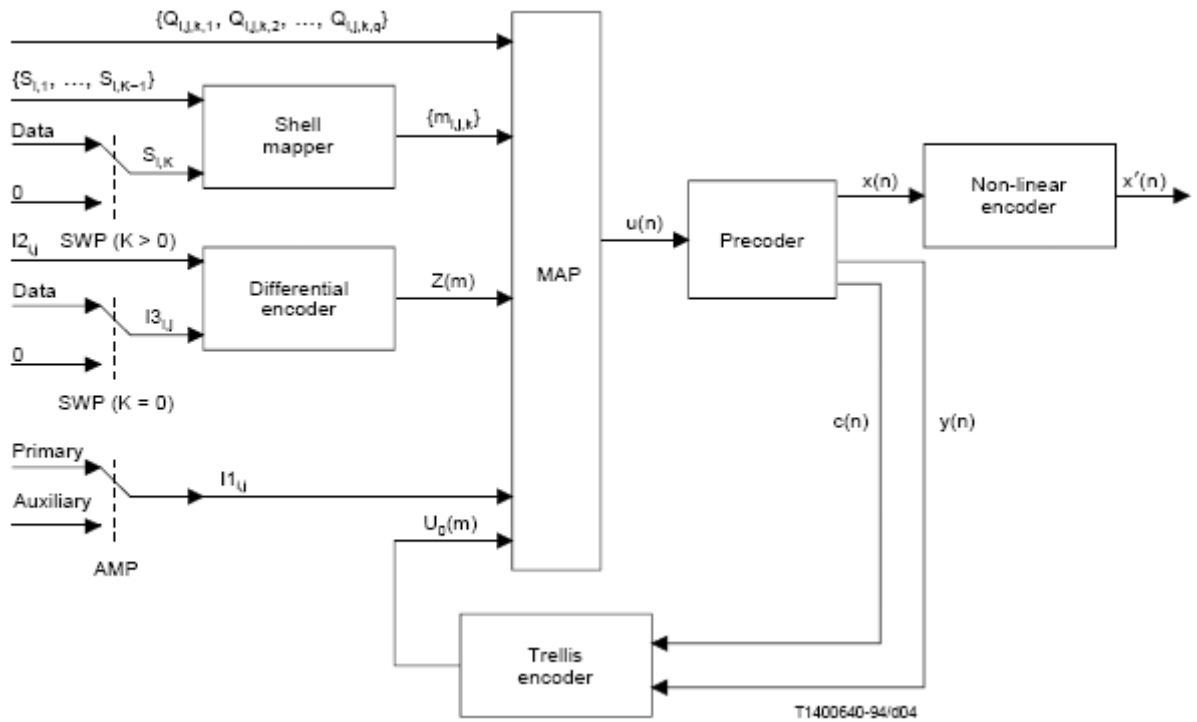


Figure 5.14.1 V.34 – Encoder block diagram

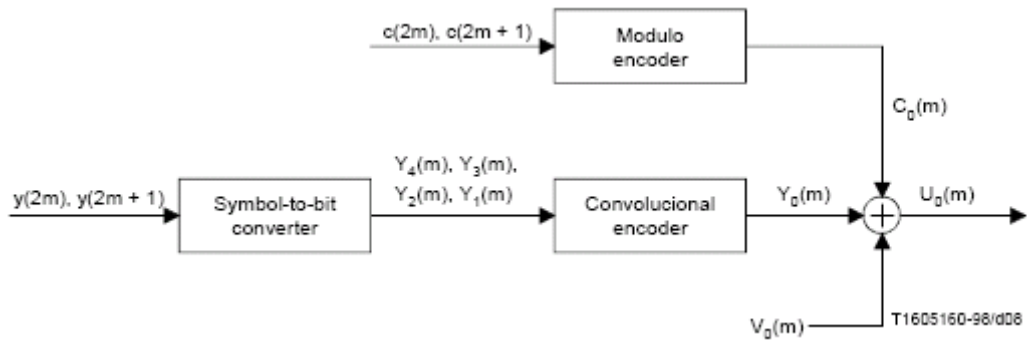


Figure 5.14.2 V.34 – Block diagram of trellis encoder

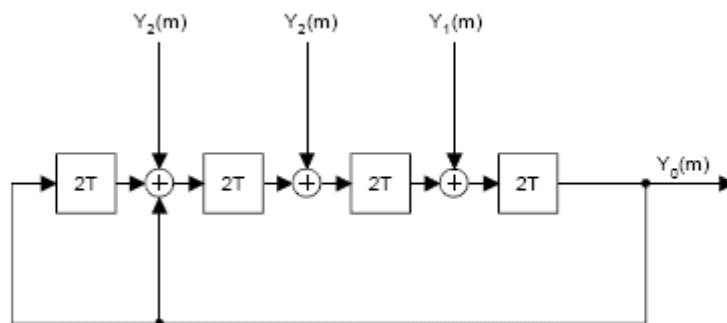


Figure 5.14.3 V.34 – 16-state convolutional encoder

5.14.2 TCM Schemes in Deep Space Applications

CCSDS 建议了 a 4D 8-PSK trellis-coded modulation for use in bandwidth-constrained communications between remote satellites and Earth stations. 它可以实现分数谱效率。

Example: Assuming the bit rate R_b of input data equal to 100 Mbps, the 4D-8PSK-TCM channel symbol rate is 50 Msps for 2 bits/channel-symbol or 40 Msps for 2.5 bits/channel-symbol.

The 4D-8PSK trellis-coded modulator consists of a serial to parallel converter, a differential coder, a 64 状态、3/4 码率的 convolutional coder, a constellation mapper and an 8PSK modulator. Spectral efficiencies of 2, 2.25, 2.5, and 2.75 bits/channel-symbol are achieved with four possible architectures of the constellation mapper. 谱效率为 2.5b/s/Hz 时的编码器结构如图 5.14.4 所示。Carrier phase ambiguity is resolved by the use of a differential coder located prior to the trellis encoder. The output switch addresses successively one of the four symbols ($Z^{(0)} - Z^{(3)}$) from the constellation mapper to the 8PSK modulator.

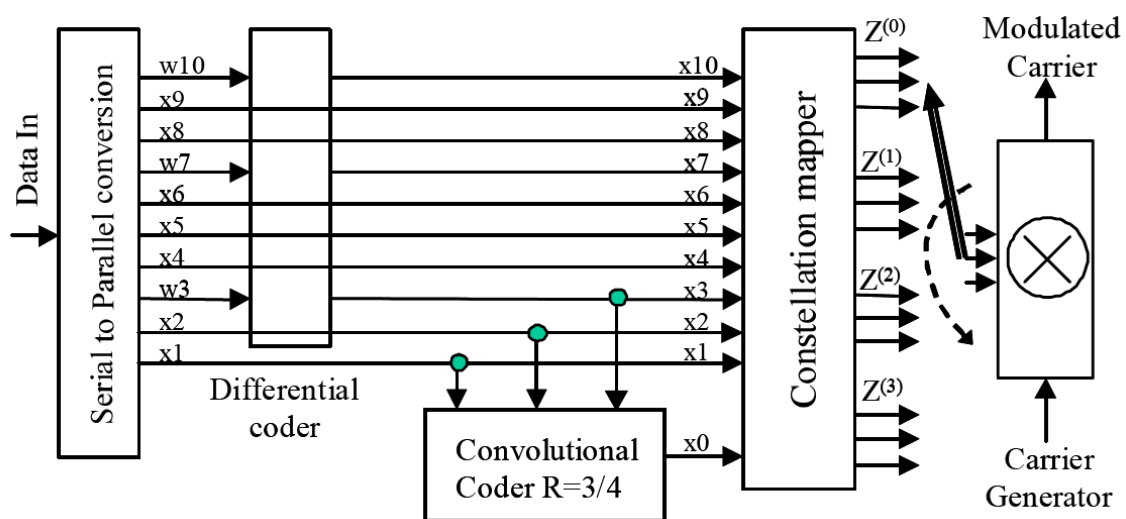
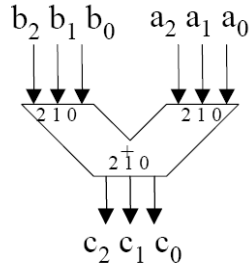


Figure 5.14.4. Coder and Mapper Implementation at 2.5 Bits/Channel-Symbol

The differential coder depicted in figure 5.14.4 is used to eliminate phase ambiguity on carrier synchronization. 在 2.5 bits/channel-symbol 时, the input bits to differential coder are w_3 , w_7 and w_{10} , and the output bits are x_3 , x_7 , and x_{10} . The structure of the modulo-8 adder is shown in figure 5.14.5; it is applicable to both the coder mapper and differential coder.



$$\begin{aligned}
 c_0 &= a_0 \oplus b_0 \text{ with carry } r_0 \\
 c_1 &= a_1 \oplus b_1 \oplus r_0 \text{ with carry } r_1 \\
 c_2 &= a_2 \oplus b_2 \oplus r_1 \\
 r_0 &= a_0 \cdot b_0 \\
 r_1 &= (a_1 \cdot b_1) + (a_1 \cdot r_0) + (b_1 \cdot r_0)
 \end{aligned}$$

图 5.14.5 modulo-8 adder

卷积编码器的结构如图 5.14.6 所示，其连接多项式为（8 进制）：h3=050, h2=024, h1=006, h0=103.

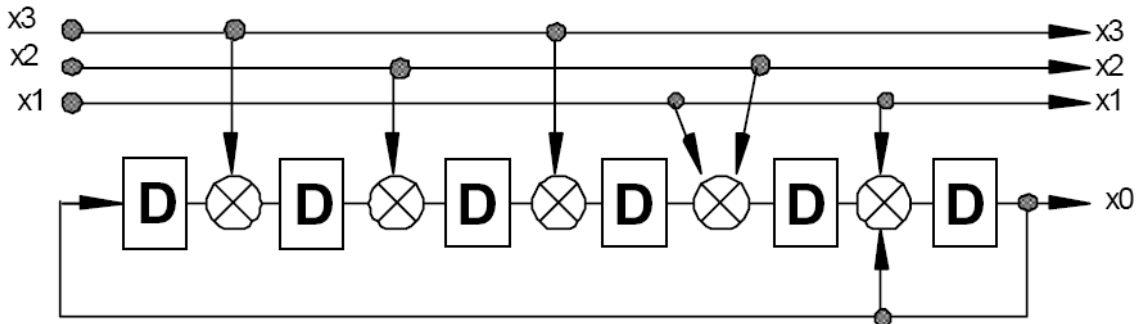
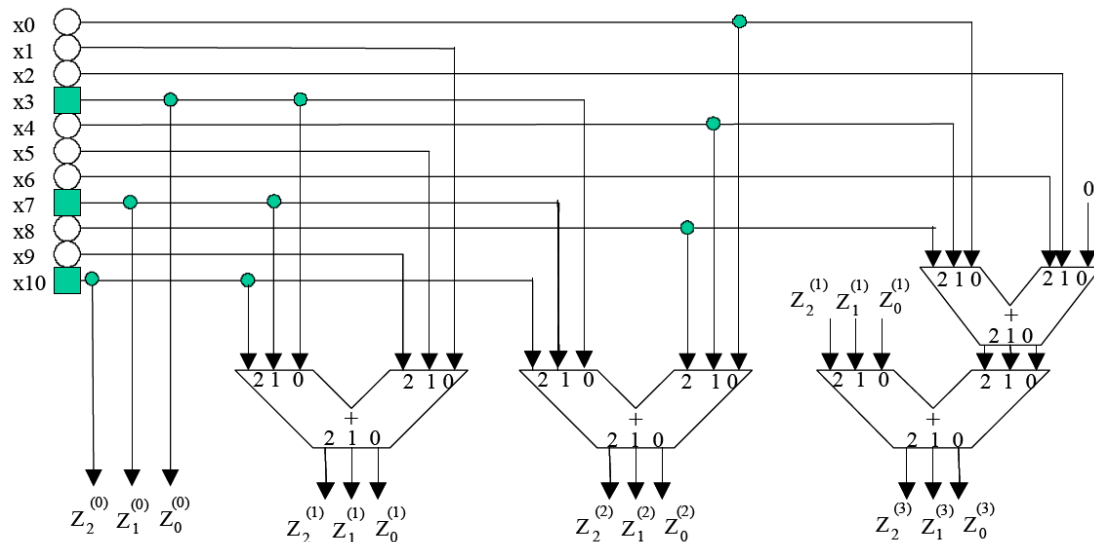


图 5.14.6. 64 状态 convolutional encoder

The constellation mapper principle is given in figures 5.14.7 for the efficiency of 2.5 bits/channel-symbol. The correspondence between the signals $Z^{(i)}$ at the input of the modular and the 8-PSK phase states of the constellations follows a natural mapping (i.e., 0, 1, 2, ..., 7).

$$\begin{bmatrix} Z^{(0)} \\ Z^{(1)} \\ Z^{(2)} \\ Z^{(3)} \end{bmatrix} = \left[\begin{matrix} 1 \\ 1 \\ 1 \\ 1 \end{matrix} \left(4x^{(10)} + 2x^{(7)} + x^{(3)} \right) + 4 \begin{bmatrix} 0 \\ x^{(9)} \\ x^{(8)} \\ x^{(9)} + x^{(8)} + x^{(6)} \end{bmatrix} + 2 \begin{bmatrix} 0 \\ x^{(5)} \\ x^{(4)} \\ x^{(5)} + x^{(4)} + x^{(2)} \end{bmatrix} + \begin{bmatrix} 0 \\ x^{(1)} \\ x^{(0)} \\ x^{(1)} + x^{(0)} \end{bmatrix} \right] \text{mod } 8$$



■ = line connected to differential coder

○ = line connected to serial-to-parallel converter or convolutional coder

Figure 5.14.7: Constellation Mapper for 2.5 Bits/Channel-Symbol

References

- [1] E. Zehavi, "8-PSK trellis codes for a Rayleigh channel," *IEEE Transactions on Communications*, vol. 40, no. 5, pp. 873–884, 1992.
- [2] G. Caire, G. Taricco, and E. Biglieri, "Bit-interleaved coded modulation," *IEEE Transactions on Information Theory*, vol. 44, no. 3, pp. 927–946, 1998.
- [3] U. Wachsmann, R. F. H. Fischer, and J. B. Huber, "Multilevel codes: Theoretical concepts and practical design rules," *IEEE Transactions on Information Theory*, vol. 45, no. 5, pp. 1361–1391, July 1999.
- [4] J. Tan and G. Stuber, "Analysis and design of symbol mappers for iteratively decoded BICM," *IEEE Transactions on Wireless Communications*, vol. 4, no. 2, pp. 662–672, 2005.
- [5] J. L. Massey, "Coding and modulation in digital communications," in *International Zurich Seminar Digital Communications, Zurich, Switzerland*, 1974.
- [6] A. Martinez, A. Guill'en i F'abregas, G. Caire, and F. Willems, "Bit-interleaved coded modulation in the wideband regime," *IEEE Transactions on Information Theory*, vol. 54, no. 12, pp. 5447–5455, December 2008.
- [7] A. Martinez, A. Guill'en i F'abregas, G. Caire, and F. Willems, "Bitinterleaved coded modulation revisited: A mismatched decoding perspective," *submitted to IEEE Transactions on Information Theory*, <http://arxiv.org/abs/0805.1327>, 2008.
- [8] X. Li, A. Chindapol, and J. A. Ritcey, "Bit-interleaved coded modulation with iterative decoding and 8 PSK signaling," *IEEE Transactions on Communications*, vol. 50, no. 8, pp. 1250–1257, 2002.
- [9] X. Li and J. A. Ritcey, "Trellis-coded modulation with bit interleaving and iterative decoding," *IEEE Journal on Selected Areas in Communications*, vol. 17, no. 4, pp.

715–724, 1999.

[10]X. Li and J. A. Ritcey, “Bit-interleaved coded modulation with iterative decoding,” *IEEE Communication Letters*, vol. 1, no. 6, pp. 169–171, November 1997.

[11]R. F. Fischer, *Precoding and Signal Shaping for Digital Transmission*. USA, New York, NY: John Wiley & Sons, Inc., 2002.